Molecular Biology of the Cell
Vol. 19, 4611–4627, November 2008

Microtubule-mediated Src Tyrosine Kinase Trafficking in Neuronal Growth Cones

Bingbing Wu,* Boris Decourt,* Muhammad A. Zabidi,* Levi T. Wuethrich,* William H. Kim,* Zhigang Zhou,† Keira MacIsaac,* and Daniel M. Suter*‡

*Department of Biological Sciences, ‡Bindley Bioscience Center, and †Department of Medicinal Chemistry and Molecular Pharmacology, Purdue University, West Lafayette, IN 47907

Submitted June 13, 2008; Revised July 30, 2008; Accepted August 13, 2008
Monitoring Editor: Paul Forscher

Src family tyrosine kinases are important signaling enzymes in the neuronal growth cone, and they have been implicated in axon guidance; however, the detailed localization, trafficking, and cellular functions of Src kinases in live growth cones are unclear. Here, we cloned two novel *Aplysia* Src kinases, termed Src1 and Src2, and we show their association with both the plasma membrane and the microtubule cytoskeleton in the growth cone by live cell imaging, immunocytochemistry, and cell fractionation. Activated Src2 is enriched in filopodia tips. Interestingly, Src2-enhanced green fluorescent protein–positive endocytic vesicles and tubulovesicular structures undergo microtubule-mediated movements that are bidirectional in the central domain and mainly retrograde in the peripheral domain. To further test the role of microtubules in Src trafficking in the growth cone, microtubules were depleted with either nocodazole or vinblastine treatment, resulting in an increase in Src2 plasma membrane levels in all growth cone domains. Our data suggest that microtubules regulate the steady-state level of active Src at the plasma membrane by mediating retrograde recycling of endocytosed Src. Expression of constitutively active Src2 results in longer filopodia that protrude from smaller growth cones, implicating Src2 in controlling the size of filopodia and lamellipodia.

INTRODUCTION

Src, Fyn, and Yes represent the main members of the Src family of protein tyrosine kinases (PTKs) in neurons (Brown and Cooper, 1996; Thomas and Brugge, 1997), and they have been implicated in several aspects of nervous system development, including neural tube formation (Thomas *et al*., 1995), axonal growth and guidance (Maness *et al*., 1996), myelination (Umemori *et al*., 1994), and synapse stability (Mohamed *et al*., 2001; Sadasivam *et al*., 2005). Although Src−/− and Yes−/− mice exhibit no detectable neurological abnormalities (Soriano *et al*., 1991; Stein *et al*., 1994), Fyn−/− mice display subtle hippocampal defects and impaired long-term potentiation (Grant *et al*., 1992). Functional redundancy among the Src family PTKs is supported by the finding that guidance of developing olfactory axons in Src−/− and Fyn−/− double knockout mice is more affected than in single knockout animals (Morse *et al*., 1998).

The neuronal growth cone is the cellular compartment in which Src PTKs mediate their guidance function. Previous biochemical and immunocytochemical studies detected Src, Fyn, and Yes in growth cones (Maness *et al*., 1988; Bixby and Jhabvala, 1993; Helmke and Pfenninger, 1995; Burden-Gulley and Lemmon, 1996). Cell culture experiments identified Src kinases as critical signaling components downstream of several axonal guidance receptors such as L1 and neural cell adhesion molecule (NCAM). For example, L1-dependent neurite outgrowth was specifically reduced in neurons from Src−/− mice, whereas NCAM-mediated neurite outgrowth was impaired in neurons from Fyn−/− mice (Beggs *et al*., 1994; Ignelzi *et al*., 1994; Maness *et al*., 1996). Furthermore, inhibition of Src activity blocked *Aplysia* growth cone steering induced by apCAM (Suter and Forscher, 2001; Suter *et al*., 2004), the *Aplysia* homologue of NCAM, while increasing laminin-mediated neurite outgrowth in chick sensory neurons (Hoffman-Kim *et al*., 2002). More recently, Src PTKs have been implicated in growth cone guidance responses to netrin, brain-derived neurotrophic factor, ephrinA, and Semaphorin 3B (Knoll and Drescher, 2004; Li *et al*., 2004; Liu *et al*., 2004; Meriane *et al*., 2004; Falk *et al*., 2005; Robles *et al*., 2005).

Thus, mounting evidence indicates that Src PTKs regulate axonal growth and guidance; however, little is known about the cell biology of Src in the growth cone, including its subcellular distribution, trafficking, and regulation as well as sites of activation and function. Such information is essential to better understand the molecular and cellular mechanisms of Src-regulated growth cone motility and guidance. Although Src is a key signaling molecule, surprisingly, its trafficking has been investigated in nonneuronal cells only recently (Bijlmakers and Marsh, 1999; Kasahara *et al*., 2004; Sandilands *et al*., 2004; Kasahara *et al*., 2007a). In addition, Src plays a role in trafficking of endosomes and macropinosomes in nonneuronal cells (Gasman *et al*., 2003; Sandilands *et al*., 2004; Kasahara *et al*., 2007b) as well as in various types of endocytosis, including internalization of the neuronal cell

This article was published online ahead of print in *MBC in Press* (http://www.molbiolcell.org/cgi/doi/10.1091/mbc.E08–06–0603) on August 20, 2008.

Address correspondence to: Daniel Suter (dsuter@purdue.edu).

Abbreviations used: ASW, artificial seawater; C, central; CSB, cytoskeleton stabilizing buffer; DIC, differential interference contrast; EGFP, enhanced green fluorescent protein; FRAP, fluorescent recovery after photobleaching; FSM, fluorescent speckle microscopy; MT, microtubule; P, peripheral; PTK, protein tyrosine kinase; RACE, rapid amplification of cDNA ends; SH, Src homology; SYF, cell line from Src/Yes/Fyn triple knockout mouse; T, transition.

adhesion molecule L1 (Schmid *et al*., 2000; Mettlen *et al*., 2006; Fessart *et al*., 2007; Kasahara *et al*., 2007b; Sverdlov *et al*., 2007).

However, Src dynamics and its regulation in live growth cones have not been investigated. For example, is Src distribution in the growth cone controlled by the cytoskeleton? Where in the growth cone is Src preferentially activated? To study localization, trafficking, and activity of Src in growth cones, we performed live cell imaging of two novel *Aplysia* Src kinases, Src1 and Src2, tagged with enhanced green fluorescent protein (EGFP) in the large growth cones of *Aplysia californica* neurons. We show that both kinases associate with the plasma membrane and the cytoskeleton in growth cones. Src2-positive endocytic vesicles and tubulovesicular structures undergo retrograde movements in the peripheral domain and bidirectional movements in the central domain in a microtubule (MT)-dependent manner. Our results indicate that the MT cytoskeleton plays an important role in regulating the steady-state levels of Src in growth cones by mediating the retrograde transport of Src endocytosed in the growth cone peripheral and transition domains. Finally, we show that constitutively active Src2 is less recycled at the plasma membrane and concentrated at filopodia tips where it controls filopodia lengths.

MATERIALS AND METHODS

Cloning of Aplysia Src1 and Src2

Aplysia Src kinases were cloned using a homology polymerase chain reaction (PCR) approach. Degenerate primers were designed based on highly conserved regions in the Src homology (SH) 3 and SH1 domains of 20 invertebrate and vertebrate Src kinases. Supplemental Table 1A contains the degenerate primer sequences. The total CNS tissue of two adult *Aplysia* (Marinus Scientific, Garden Grove, CA) was homogenized in TRIzol (Invitrogen, Carlsbad, CA), and total RNA was extracted following the manufacturer's instructions. Total RNA was then reverse transcribed using the SuperScript II reverse transcription kit (Invitrogen) and random hexamer nucleotides. PCR reactions with *Taq* polymerase (Invitrogen) and two different reverse primers resulted in two Src tyrosine kinase sequences (465 and 636 base pairs, respectively), termed Src1 and Src2. Additional 5′ and 3′ sequence information was obtained by rapid amplification of cDNA ends (RACE) reactions by using the Smart RACE cDNA kit (Clontech, Mountain View, CA) and the primers listed in Supplemental Table 1B. RACE products were subcloned into TOPO-TA vector (Invitrogen) for sequencing (Purdue Genomics Core Facility, West Lafayette, IN). Full-length Src1 and Src2 sequences were confirmed by PCR using Pfx DNA polymerase (Invitrogen) and gene-specific primers at the 5′ and 3′ ends of Src1 and Src2, respectively. Sequence alignments and phylogenetic tree analysis were performed using Vector NTI suite 8.0 software (Invitrogen). Src1 and Src2 nucleotide sequences have been deposited with the following GenBank accession numbers: FJ172681 (for Src1) and FJ172682 (for Src2).

EGFP Expression Constructs of Aplysia Src1 and Src2

We used the pRAT vector (kindly provided by Dr. Steve Goldstein, Yale University, New Haven, CT) to express Src1- and Src2-EGFP fusion proteins as well as untagged and mutant Src constructs in *Aplysia* bag cell neurons. The EGFP-sequence was first subcloned from pNEX3-EGFP (kindly provided by Dr. Wayne Sossin, McGill University, Montreal, QC, Canada) into pRAT vector by using EcoR1 restriction sites. Src1 and Src2 were amplified by PCR using *Aplysia* total nervous system cDNA, Platinum Pfx DNA polymerase (Invitrogen), and the primers indicated in the Supplemental Table 1C, which include AgeI sites. PCR products were subcloned into the pRAT-EGFP plasmid via AgeI sites. In the resulting Src1- and Src2-EGFP fusion constructs, the EGFP-tag was connected to the C terminus of Src1 and Src2 via the linker GGGGGPVAT. Untagged Src1 and Src2 were subcloned into pRAT by PCR using pRAT-Src1-EGFP and pRAT-Src2-EGFP as templates and the primers listed in Supplemental Table 1D, which introduced EcoRI and SacII restriction sites for Src1 and Src2 subcloning, respectively.

Src1 and Src2 cDNAs were also subcloned into pIZ/V5–6His plasmid (Invitrogen). cDNAs were amplified from pRAT constructs by using the Advantage II polymerase mix (Clontech) and the primers listed in Supplemental Table 1E, which contain an SpeI and an XhoI site, respectively. To prepare EGFP-tagged Src constructs in pIZ/V5–6His, Src1-EGFP in pRAT and Src1 in pIZ/V5–6His were amplified in SCS 110 Dam$^-$ bacteria and digested with BclI and SacII. The pRAT fragment containing the 3′ sequence of Src1 fused to EGFP was then ligated into the pIZ/V5–6His plasmid containing Src1. Similarly, Src2-EGPF in pRAT and Src2 in pIZ/V5–6His were amplified in DH5α bacteria and digested with NdeI and SacII. The 3′ segment of Src2 fused to EGFP was ligated into the Src2-containing pIZ/V5–6His plasmid. All constructs were confirmed by sequencing.

Site-directed Mutagenesis

Membrane defective G2A mutants, kinase dead (Src2 K286M), and tail regulation (Src2 Y518F) mutants were made using QuikChange II site-directed mutagenesis kit (Stratagene, La Jolla, CA) by using the corresponding wild-type constructs as templates. All constructs were verified by sequencing.

Structure Modeling of Aplysia Src2-EGFP Fusion Protein

Structural models for the *Aplysia* Src2-EGFP fusion protein were generated by homology modeling for Src without the N terminus and the EGFP protein, and molecular mechanics-based modeling for the linker region. Homology modeling was executed with the program Modeler 9v1, and sequence alignments were carried out using BLAST with default settings for the BLOSUM62 matrix analysis. The templates for the active and inactive forms of *Aplysia* Src2 were the structures of activated (Protein Data Bank [PDB] code 1Y57) and down-regulated (PDB code 2SRC) human Src, respectively. The template for EGFP was the GFP protein (PDB code 1EMM). Twenty structures for each protein were generated, and the structure with the best score based on the main chain dihedral angles according to a Ramachandran analysis was used for the fusion protein. The three-dimensional structure of the nine-residue linker (GGGGGPVAT) between Src2 and EGFP, and seven residues (MVSKGEE) at the N terminus of EGFP, which do not align with residues in green fluorescent protein (GFP) and are therefore not in the GFP crystal structure, were modeled using the Protein Builder module of the program MOE (Chemical Computing Group, Montreal, Quebec, Canada). The main chain conformation was evaluated from a Ramachandran plot of the linker and the C-terminal residues of Src2. The linker was then connected to the GFP protein by modeling a low-energy peptide bond between the N terminus of GFP and the C terminus of the linker.

Aplysia Bag Cell Neuronal Cultures

Aplysia bag cell neurons were cultured in L15 medium (Invitrogen) supplemented with artificial seawater (ASW; 400 mM NaCl, 9 mM $CaCl_2$, 27 mM $MgSO_4$, 28 mM $MgCl_2$, 4 mM L-glutamine, 50 μg/ml gentamicin, and 5 mM HEPES, pH 7.9) on coverslips coated with 20 μg/ml poly-L-lysine (70–150 kDa) as described previously (Forscher *et al*., 1987; Suter *et al*., 1998). Chemicals were from Sigma-Aldrich (St. Louis, MO) unless otherwise noted.

Src Expression in Aplysia Neurons

Src1 and Src2 wild-type and mutant constructs with and without EGFP were expressed by microinjection of in vitro-transcribed mRNA into bag cell neuronal cell bodies typically 1 d after cell plating. mRNA was prepared using the mMESSAGE mMACHINE T7 in vitro transcription kit (Ambion, Austin, TX). After lithium chloride precipitation and resuspension at 2–4 μg/μl in TE buffer, mRNA was incubated at 65°C for 5 min and then coinjected together with 2.5 μg/μl Texas Red dextran (3 kDa; Invitrogen) into the cell bodies of *Aplysia* bag cell neurons by using the NP2 micromanipulator and FemtoJet microinjection system (Eppendorf North America, New York, NY). Expression of EGFP proteins could be observed as early as 5 h after injection. Neurons were typically imaged 18–24 h after mRNA injection.

For Src/MT fluorescent speckle microscopy (FSM) dual-channel imaging, 5 μg/μl Src-EGFP mRNA was mixed with 1 μg/μl rhodamine-tubulin (Cytoskeleton, Denver, CO) in tubulin injection buffer (100 mM 1,4-piperazinediethanesulfonic acid [PIPES], pH 6.8, 1 M $MgCl_2$, and 1 mM EGTA) at a 1:1 volume ratio. The RNA/tubulin mixtures were centrifuged at 10,000 $\times$ *g* for 20 min at 4°C before loading into microcapillary needles. For endocytic marker uptake experiments, *Aplysia* bag cell neurons expressing Src2-EGFP were incubated with either 2 mg/ml Texas Red-dextran (70 kDa, neutral; Invitrogen) or 10 μM *N*-[3-triethylammoniumpropyl]-4-[*p*-diethylaminophenylhexatrienyl] pyridinium dibromide (FM4-64) (Invitrogen) in L15-ASW medium. The medium containing the fluorescent endocytic marker was spun at 10,000 $\times$ *g* for 20 min at room temperature (RT) before Src2-EGFP–expressing neurons were incubated for 5 min (dextran) and 1 min (FM4-64) followed by three washes with 1 ml of L15-ASW each. Dual-channel (Src2-EGFP/endocytic marker) time-lapse images were taken immediately after fluorescent marker incubation.

Src Expression in Cell Lines

Chinese hamster ovary (CHO) cells (American Type Culture Collection, Manassas, VA) and SYF cells (fibroblast cell line from Src, Yes, Fyn deficient mice; American Type Culture Collection) were cultured in DMEM-Ham's F-12 (Invitrogen) including 10% fetal bovine serum (FBS; HyClone Laboratories, Logen, UT) and 100 U/ml penicillin/0.1 mg/ml streptomycin (Invitrogen). Cells were replated on 60-mm Petri dishes 1 d before Lipofectamine 2000-mediated transfection of various Src constructs in pRAT was performed. After 1 d of transfection, Src-expressing CHO and SYF cells were lysed and ana-

lyzed by Western blotting. Sf9 insect cells were cultured in serum-free Sf900 II medium (Invitrogen). Cells were transfected in 35-mm Petri dishes at 80% confluence by using Cellfectin (Invitrogen) and 5 μg pIZ/V5–6His DNA. After 48 h of Src expression, Sf9 cells were centrifuged for 5 min at 1000 $\times$ *g*, and cell pellets were lysed and analyzed by Western blotting.

Peptide Antibodies

Polyclonal anti-*Aplysia* Src1 and Src2 antibodies (Pacific Immunology, Ramona, CA) were raised against peptides derived from respective N-terminal regions: GEKGSSTKYLPDPFQG (amino acids [aa] 10–25) for the rabbit anti-Src1 antibody; SNTAGDASPSHRLAENG (aa 14–30) for the goat anti-Src2 antibody. The sequence around the autophosphorylation site ARVIKEDE(pY)EARVG (aa 399–412) was used for the rabbit anti-pSrc2 (activated Src2) antibody. The pSrc2 antibody was first purified against the nonphosphorylated and then the phosphorylated peptide. Affinity-purified antibody stock solutions were prepared at 1 mg/ml in phosphate-buffered saline (PBS)/0.01% NaN_3. To reduce binding to unspecific targets in *Aplysia* tissue, antibodies were first absorbed two times against *Aplysia* CNS proteins separated by SDS-polyacrylamide gel electrophoresis (PAGE) and transferred onto polyvinylidene fluoride membranes. The rabbit anti-active human Src antibody (Src PY418) was purchased from BioSource International (Invitrogen). Peptide blocking control experiments for Western blotting and immunocytochemistry were carried out by preincubation of antibody stock solutions (1 mg/ml in PBS), with an equal volume of the cognate or a control peptide (5 mg/ml in PBS) for 2 h at RT before antibody dilutions were prepared as described below.

Western Blotting

Total *Aplysia* CNS tissue was cut into small pieces and incubated in 2 ml of lysis buffer per animal (50 mM Tris-HCl, pH 7.5, 150 mM NaCl, 2 mM EDTA, 2 mM EGTA, 1% Triton X-100, 0.5 mM Pefabloc SC Plus [Roche Diagnostics, Indianapolis, IN], 1% protease inhibitor cocktail, 20 mM β-glycero-phosphate, 10 mM NaF, and 1 mM Na_3VO_4) for 20 min on ice, and then it was homogenized for 1 min. Homogenized tissue was cleared at 10,000 $\times$ *g* for 20 min at 4°C. For Src inhibitor experiments, the lysis buffer was modified the following way: 20 mM HEPES, pH 7.5, was used instead of 50 mM Tris-HCl, pH 7.5; 1 mM EGTA instead of 2 mM EDTA/2 mM EGTA. The buffer was supplemented with either 25 μM PP2 (BIOMOL Research Laboratories, Plymouth Meeting, PA), PP3 (Calbiochem, San Diego, CA), or dimethyl sulfoxide (DMSO). Lysates from CHO, SYF, and Sf9 cells expressing different Src constructs were prepared by incubating confluent cells in 60-mm Petri dishes with the lysis buffer described for the CNS tissue, including 5 mM EDTA/5 mM EGTA. Lysed cells were incubated for 20 min on ice, and then they were cleared as described above. Twenty micrograms of *Aplysia* CNS and 15 μg of cell line lysate protein per lane were separated on 10% SDS-polyacrylamide gels and transferred to polyvinylidene fluoride membranes (Bio-Rad, Hercules, CA). After blocking with 10% FBS/PBS for 1 h at RT, membranes were probed with primary Src antibodies at 1:500 or mouse anti-α-tubulin (clone B-5-1-2; Sigma-Aldrich) at 1:1000 in 5% FBS/PBS/0.05% Tween 20 overnight at 4°C. After washes with PBS and PBS/0.1% Tween 20, secondary antibodies conjugated to either Alexa 680 (Invitrogen) or IRDye 800 (Rockland Immunochemicals, Gilbertsville, PA) were incubated at 1:5000 in 5% FBS/PBS/0.05% Tween 20/0.01% SDS for 1 h at RT. After additional washes with PBS and PBS/0.1% Tween 20 the fluorescent signal was detected by an Odyssey infrared detection system (LI-COR Biosciences, Lincoln, NE). For probing of multiple antibodies (e.g., Src2, pSrc2, and tubulin antibody in Supplemental Figure S4D), membranes were stripped with 62.5 mM Tris-HCl, 2% SDS, and 100 mM β-mercaptoethanol for 30 min at 60°C, followed by washes with PBS and PBS/0.1% Tween 20 before the next antibody incubation. Src2 and pSrc2 signals were detected together using two different fluorescently labeled secondary antibodies. Band intensities were analyzed with the Odyssey software (LI-COR Biosciences).

Preparation of Microtubule (MT)-enriched CNS Fraction

MT-enriched fractions were prepared from *Aplysia* CNS tissues by using a modified protocol by R. Vallee and G. Bloom (Vallee, 1982; Vallee and Bloom, 1983). The *Aplysia* CNS tissue of four animals was homogenized in 4 ml of MT homogenization buffer (100 mM K-PIPES, pH 6.8, 1 mM $MgSO_4$, 1 mM EGTA, 1 mM guanosine triphosphate, 0.5 mM Pefabloc SC Plus, 1% Protease Inhibitor Cocktail, 20 mM β-glycero-phosphate, 10 mM NaF, and 1 mM Na_3VO_4) for 1 min on ice. The homogenized tissue was centrifuged at 30,000 $\times$ *g* for 30 min at 4°C. The supernatant (S1) was spun at 135,000 $\times$ *g* for 90 min at 4°C. The supernatant (S2) was warmed up to RT and supplemented with glycerol to a final concentration of 1 M. The S2 supernatant was split up equally into two parts: one part (S2T) was treated with 20 μM taxol, and the other part (S2C) with the corresponding amount of the drug vehicle DMSO for 20 min at 37°C. The samples were then transferred onto 1.5 ml of 20% sucrose cushions in MT homogenization buffer including 1 M glycerol and the corresponding MT drugs. Samples were spun at 100,000 $\times$ *g* for 30 min at 30°C. The pellets (P3T, P3C) were resuspended with 1/10 volume of supernatants (S3), whereas P1 and P2 were resuspended with the same volume as the corresponding supernatant. Equal volumes of each fraction were loaded onto 10% SDS-PAGE, followed by silver staining and Western blotting by using mouse anti-α-tubulin at 1:100,000 or rabbit anti-pSrc2 at 1:1000 and the SuperSignal West Pico ECL detection system (Pierce Chemical, Rockford, IL). Scanned films were quantified using Odyssey software.

Immunocytochemistry

Aplysia bag cell neurons were fixed with 3.7% formaldehyde/400 mM sucrose/ASW for 30 min, and then they were permeabilized with 0.05% saponin in fixative for 10 min and washed with PBS containing 0.005% saponin (wash buffer). The whole staining protocol was carried out at RT. For Src1/Src2 and Src2/pSrc2 double labelings, 1% glutaraldehyde was included in the fixation solution. In this case, after permeabilization cells were incubated twice for 15 min with 0.1% sodium borohydride in wash buffer. Alexa 488-phalloidin (Invitrogen) was used for F-acting labeling. After blocking with 10% horse serum in wash buffer for 30 min, all Src primary antibodies were incubated at 1:250 in blocking solution for 45 min. Mouse anti-α-tubulin was diluted 1:2000 in wash buffer only. Corresponding Alexa 488-, 568-, and 647-conjugated goat anti-rabbit, goat anti-mouse, and donkey anti-goat immunoglobulin G (IgG) secondary antibodies (Invitrogen) were incubated at 1:400 in wash buffer for 30 min. After washes, cells were inspected by fluorescent microscopy in 20 mM n-propyl-gallate in PBS/80% glycerol, pH 8.5. For live cell extraction, cells were washed with a Ca^{2+}-free ASW (15 mM HEPES, pH 7.9, 100 mM NaCl, 10 mM KCl, 5 mM $MgCl_2$, 60 g/L-glycine, and 5 mM EGTA) for 2 min, and then they were extracted with 1% Triton X-100 in a cytoskeleton stabilizing buffer (CSB; 80 mM PIPES, pH 7.5, 1 mM $MgCl_2$, 5 mM EGTA, 4% polyethylene glycol, 10 μM taxol, and 1 μM phalloidin) for 1 min, washed with CSB, and then fixed with CSB containing 3.7% formaldehyde for 30 min.

Microscopy and Image Analysis

All images were acquired on a Nikon TE2000 Eclipse inverted microscope either with a 60$\times$ (1.4 numerical aperture [NA]) oil immersion objective (with additional 1.5$\times$ magnification lens) or with a 100$\times$ (1.45 NA) oil immersion objective using a Cascade II charge-coupled device camera (Photometrics, Tucson, AZ) controlled by MetaMorph 7 software (Molecular Devices, Sunny Vale, CA). Fluorescent illumination was provided by an X-cite 120 metal halide lamp (EXFO, Quebec, QC, Canada) and appropriate filter sets (Chroma Technology, Brattleboro, VT). Live cell imaging was performed at RT in ASW supplemented with 2 mg/ml bovine serum albumin, 1 mg/ml L-carnosine, and 0.25 mM vitamine E. Fluorescent images were taken at 10-s intervals by using 300- to 500-ms exposure times. For fluorescent recovery after photobleaching (FRAP) experiments, growth cones expressing either Src1- or Src2-EGFP were bleached for 10 s in a circular area of 10 μm diameter in the P domain by using a 20-mW 488-nm argon laser (Melles Griot, Carlsbad, CA) connected with a fiber optics cable to a laser port of a TE2000 microscope. Two to three s after bleaching, fluorescence recovery was monitored by epi-illumination using the standard fluorescein isothiocyanate (FITC) filter set, taking images every 500 ms.

MetaMorph 7 was used for the analysis of fluorescence intensity, morphology, rate of movements and colocalization; for processing of MT FSM and EGFP time-lapse sequences; and for making of movies and montages. For determining Src levels in specific growth cone domains, the mean intensity value in the region of interest was background subtracted and averaged over 20–100 growth cones. Only Src-EGFP puncta that could be clearly tracked for at least 1 min were included in the movement analysis. To determine the percentage of Src/MT colocalization in Figure 6, both Src2 and MT images were processed with an unsharp mask filter and then thresholded. A region of interest was drawn with MetaMorph in the P region and T zone where individual MTs could be clearly identified. Using the MetaMorph "Measure colocalization" tool, we determined two values: 1) the percentage of area of thresholded Src2 signal that overlaps with the thresholded MT area and 2) the percentage of thresholded MT area of the total area in the region of interest. If the percentage of Src2 area overlapping with MTs (1) is higher than the percentage of MT area (2), this suggests that Src2-MT overlap is not purely coincidental. Fluorescent recovery in FRAP experiments was plotted in percentage of prebleach intensity values after background correction as a function of time. The two-dimensional diffusion coefficient (D) was obtained using the equation $D = r^2/4\tau$ (r is the radius of bleached area, and τ is the diffusion time). Adobe Photoshop CS3 (Adobe Systems, Mountain View, CA) was used for image processing of still images.

RESULTS

Aplysia Src1 and Src2 Are Two Novel Invertebrate Src PTKs

To investigate trafficking, activation, and functions of Src PTKs in live growth cones, we developed new molecular tools specific to *Aplysia californica* Src family kinases. Because no Src PTKs have been characterized in this species thus far, we cloned two novel cDNAs by using a PCR homology

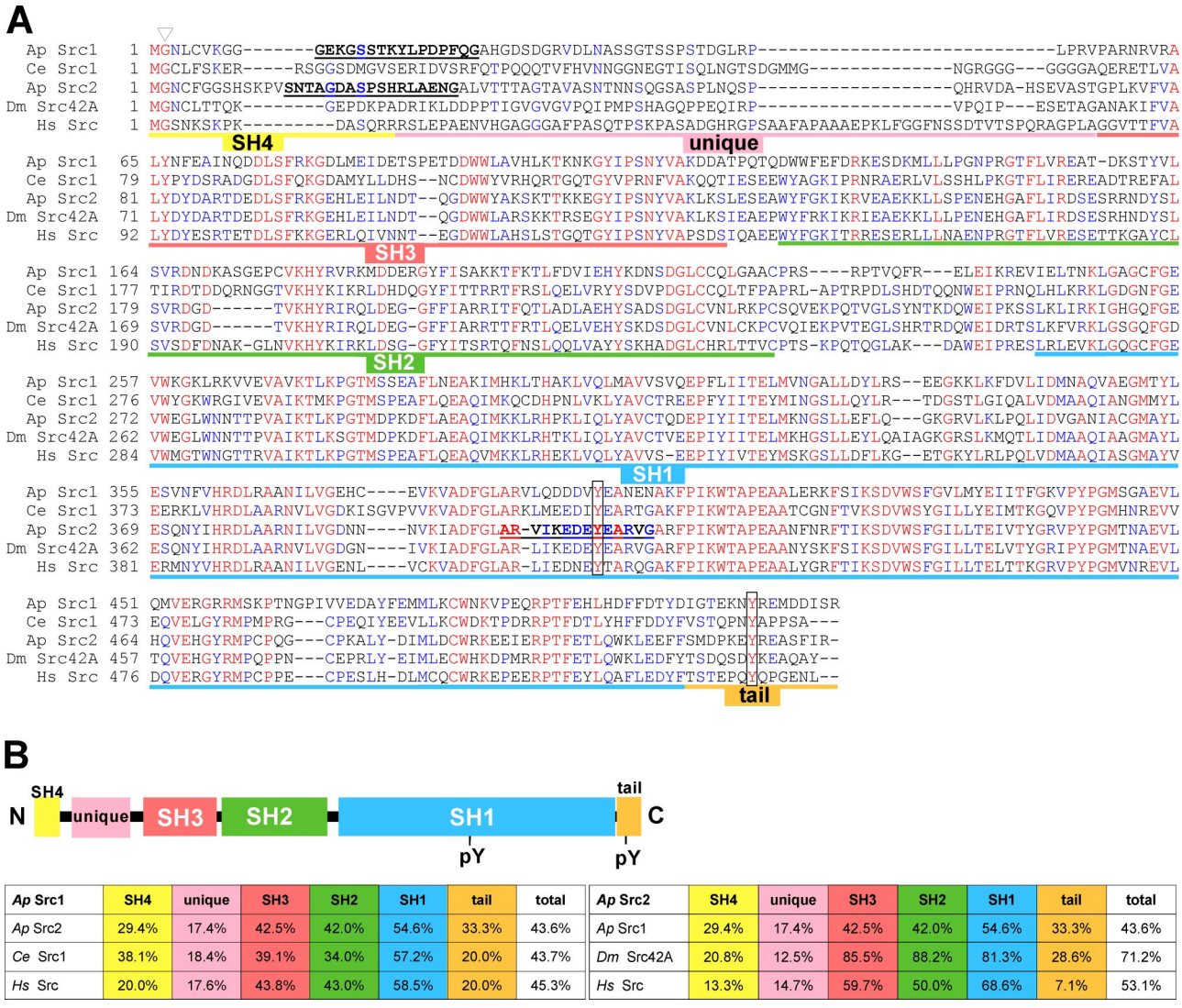

Ap Src1	SH4	unique	SH3	SH2	SH1	tail	total
Ap Src2	29.4%	17.4%	42.5%	42.0%	54.6%	33.3%	43.6%
Ce Src1	38.1%	18.4%	39.1%	34.0%	57.2%	20.0%	43.7%
Hs Src	20.0%	17.6%	43.8%	43.0%	58.5%	20.0%	45.3%

Ap Src2	SH4	unique	SH3	SH2	SH1	tail	total
Ap Src1	29.4%	17.4%	42.5%	42.0%	54.6%	33.3%	43.6%
Dm Src42A	20.8%	12.5%	85.5%	88.2%	81.3%	28.6%	71.2%
Hs Src	13.3%	14.7%	59.7%	50.0%	68.6%	7.1%	53.1%

Figure 1. *Aplysia* Src1 and Src2 are two novel Src family PTKs. (A) Amino acid sequence alignment of *A. californica* (Ap) Src1 and Src2 with *C. elegans* (Ce) Src1, *D. melanogaster* (Dm) Src42A, and *Homo sapiens* (Hs) Src. Identical amino acids in red; amino acids conserved in at least three sequences in blue. Domains are assigned based on human Src. Triangle, conserved glycine at position 2. Boxes, conserved tyrosine residues at the autophosphorylation site (Src1 Y394, Src2 Y407) and in the C-terminal tail (Src1 Y509, Src2 Y518). Bold and underlined: peptide sequences that were used for antibody generation. (B) Domain organization of Src PTKs. Left, percentage of amino acid identities between *Aplysia* Src1 and Src2, *C. elegans* Src1, and human Src by domains and as full-length protein. Right, percentage of amino acid identities between *Aplysia* Src2 and Src1, *D. melanogaster* Src42A, and human Src.

approach and named them *Aplysia* Src1 and Src2. The deduced amino acid sequences of both Src1 (517 aa) and Src2 (525 aa) contain the typical domains of Src family PTKs, including the N-terminal Src homology 4 (SH4) and unique domains, followed by the SH3, SH2, and SH1 (kinase) domains and the C-terminal tail with regulatory function (Figure 1, A and B). It is interesting to note that *Aplysia* Src2 has a higher sequence identity to human Src (53.1%) than to *Aplysia* Src1 (43.6%; Figure 1B). As with other Src kinases, Src1 and Src2 are the least conserved in the N-terminal SH4 and unique domains, as well as in the C-terminal tail, whereas the SH3, SH2, and SH1 domains exhibit higher sequence identities across species (Figure 1B). An exception is the glycine at position 2, which can be myristoylated in all Src kinases (arrowhead in Figure 1A). Both Src1 and Src2 contain the highly conserved tyrosine residue in the kinase domain (Src1 Y394, Src2 Y407, respectively) that can be autophosphorylated to achieve maximum kinase activity (box in Figure 1A). The C-terminal tail contains the canonical tyrosine residue that can be phosphorylated by the C-terminal Src kinase (Src1 Y509, Src2 Y518, respectively) to inactivate Src (box in Figure 1A). Phylogenetic tree analysis indicates that *Aplysia* Src1 and Src2 belong to two distinct subfamilies of invertebrate Src PTKs (Supplemental Figure S1). *Aplysia* Src1 forms a subfamily with *Caenorhabditis elegans* Src1 and *Drosophila melanogaster* Src64B that changed the most from the common ancestor gene. *Aplysia* Src2 belongs to a larger subfamily that includes *D. melanogaster* Src42A, *C. elegans* Src2, and various Src PTKs from marine and freshwater sponges.

Src1 and Src2 Are Present in All Growth Cone Domains

To study the distribution of *Aplysia* Src1 and Src2 in growth cones, we designed polyclonal antibodies against unique

peptide sequences in the N terminus of both kinases, as well as against the autophosphorylation site of Src2 to detect activated Src2 (pSrc2; Figure 1A). Because a corresponding pSrc1 antibody did not detect any active Src1 signals in Western blots (unpublished data), we focused the Src activation-related experiments on Src2. We tested the specificity of our peptide antibodies by immunoblotting of heterologously expressed and endogenous *Aplysia* Src proteins (Supplemental Figure S2). The antibodies recognized the corresponding recombinant Src or Src-EGFP proteins at the expected molecular weight (60 and 90 kDa, respectively), with no cross-reactivity (Supplemental Figure S2A). The polyclonal antibody against activated human Src, Src PY418, which we used in previous studies on *Aplysia* growth cones (Suter and Forscher, 2001; Suter *et al*., 2004), specifically detects *Aplysia* Src2 and not Src1. The specificity of our Src antibodies for endogenous Src1, Src2, and activated Src2 was confirmed by immunoblotting of *Aplysia* CNS protein lysates (Supplemental Figure S2, B and C). The Src1 band runs at 62 kDa, slightly higher compared with the Src2 band at 60 kDa. Peptide preincubation completely abolished the signal. Pretreatment of CNS tissue with 25 μM of the Src family-selective inhibitor PP2 but not the inactive analogue PP3 for 20 min resulted in a 54% reduction of Src2 activation levels compared with untreated samples (Supplemental Figure S2C). Thus, these polyclonal antibodies are valid tools to discriminate between Src1 and Src2 as well as activated Src2.

Immunolabeling with these Src1- and Src2-specific antibodies revealed a punctate distribution of both kinases throughout the central (C) domain, transition (T) zone, and peripheral (P) domain of *Aplysia* growth cones (Figure 2). The punctate Src-staining pattern likely results from Src associated with residual plasma membrane after saponin extraction, vesicles, and the cytoskeleton (see below). Src1 and Src2 distributions were similar in these three domains; however, the C domain sometimes had higher signals (e.g., Figure 2B). Although overall Src1 and Src2 distributions looked similar, double labeling revealed that only a small percentage of puncta were both Src1 and Src2 positive (white arrowhead and inset in Figure 2D). Increased levels of activated Src2 were detected at the tips of filopodia (white arrows and inset in Figure 2E). In agreement with our previous study (Suter and Forscher, 2001), the same staining pattern was observed with the Src PY418 antibody, which detects activated Src2 (Figure 2F and Supplemental Figure S2A). Preincubation of the individual Src antibodies with their specific peptide strongly reduced the immunofluorescence signal by 40–50% compared with controls, and no staining was detected when primary antibodies were omitted, confirming the specificity of immunofluorescence data (Supplemental Figure S3). Double labeling with Src2 and pSrc2 antibodies revealed that a significant portion of Src2-puncta was pSrc2 positive (white arrowheads and inset in Figure 2G). To test the specificity of the pSrc2 immunolabeling, we treated *Aplysia* neurons with the Src family-selective inhibitor PP2 (25 μM for 20 min), which resulted in a significant decrease in the density and intensity of puncta, particularly at filopodia tips (Figure 2H). Thus, PP2 pretreatment reduced Src2 activation levels in growth cones to a similar extent (57%; Figure 2I) as in *Aplysia* CNS extracts (54%; Supplemental Figure S2C), confirming the specificity of our pSrc2 antibody. In summary, *Aplysia* Src1 and Src2 have a similar distribution in growth cones, but they exhibit

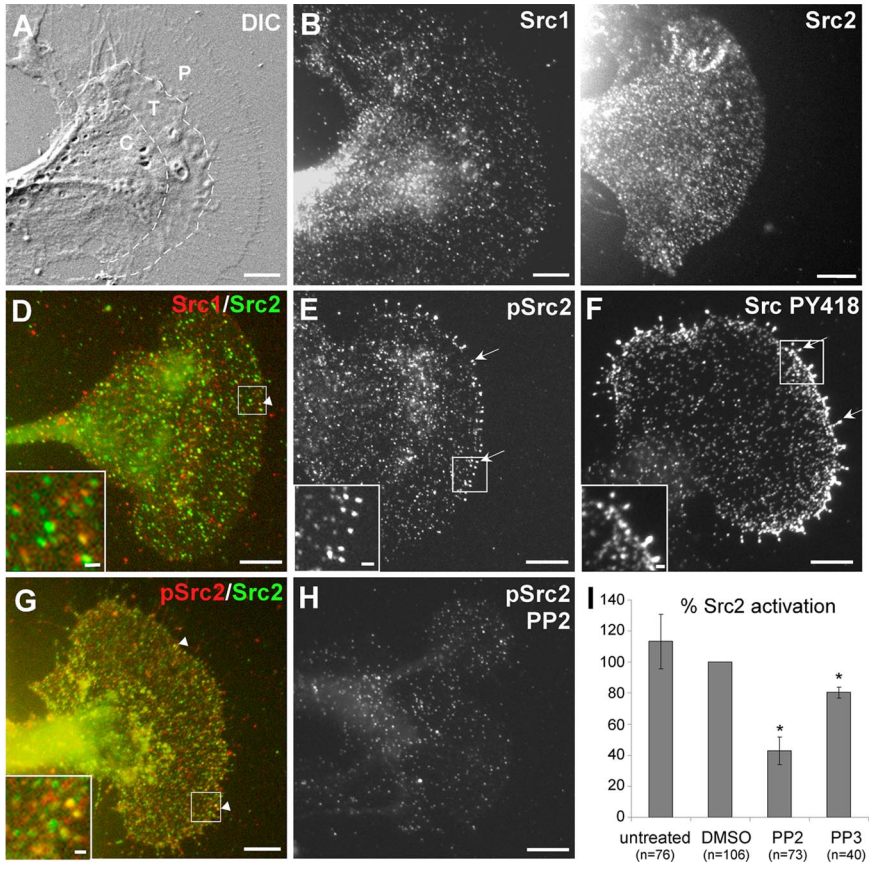

Figure 2. Localization of *Aplysia* Src1 and Src2 in growth cones. (A) DIC image of *Aplysia* bag cell neuronal growth cone after fixation. C and P domain plus T zone are indicated. (B) Src1 immunolabeling of the growth cone shown in A reveals a punctate distribution of Src1 in all three domains with elevated signals in the C domain. (C) Different growth cone stained for Src2. (D) Overlay of Src1 (red) and Src2 (green) double labeling revealed only little colocalization (arrowhead and inset showing boxed region of interest enlarged). (E) Activated Src2 labeled by pSrc2 is concentrated at filopodia tips (arrows and inset). (F) A similar staining pattern was observed with the Src PY418 antibody. (G) Overlay of total Src2 (green) and activated Src2 (red) double-labeling (arrowheads and inset). (H) Pretreatment of neurons with 25 μM PP2 for 20 min reduced the pSrc2 signal in all growth cone regions, particularly at filopodia tips. Bars, 10 μm; 1 μm in insets of D–G. (I) Quantification of three independent experiments revealed a 57% decrease of pSrc2 signal in the P domain of PP2-treated growth cones compared with DMSO-treated cells (n is number of growth cones; *t* test: $p < 0.005$ for PP2 vs. DMSO; asterisk), whereas PP3 caused a smaller decrease of 20% ($p = 0.005$ for PP3 vs. DMSO; Figure 2I). Src2 activation levels are given in percentage of the DMSO condition as mean values ± SEM.

very little colocalization. Furthermore, activated Src2 is enriched in filopodial tips.

Src1- and Src2-EGFP Localize to the Plasma Membrane of Growth Cones

A few very recent studies have reported live cell imaging of Src in nonneuronal cells (Carreno *et al*., 2000; Sandilands *et al*., 2004; Newsome *et al*., 2006; Kasahara *et al*., 2007a,b; Shvartsman *et al*., 2007); however, no data are available on Src dynamics and trafficking in live growth cones. Therefore, we constructed EGFP-fusions of both *Aplysia* Src1 and Src2. To avoid potential interference with N-terminal myristoylation and related membrane localization (Cross *et al*., 1984), we fused the EGFP sequence to the C terminus of both Src1 and Src2 by using a flexible glycine-rich linker (GGGGGPVAT). To test whether the C-terminal EGFP-tag could interfere with the activation or negative tail regulation of Src1- and Src2-fusion proteins (Thomas and Brugge, 1997; Xu *et al*., 1999), we used 1) structural modeling and 2) a biochemical and 3) functional approach focusing on Src2 (Supplemental Figure S4 and Figure 8).

Structural modeling of the *Aplysia* Src2-EGFP fusion protein suggests that the C-terminal tail of Src2, 9-residue linker, plus N-terminal EGFP residues are long and flexible enough to spatially separate Src2 and EGFP and to allow interaction of the tyrosine-phosphorylated tail with the SH2 domain without interference by the EGFP moiety (Supplemental Figure S4, A–C). In a second approach, we assessed the activation state of wild-type Src2 and various mutants with and without the EGFP-tag by expressing them in Sf9 cells followed by immunoblotting with both Src2 and pSrc2 antibodies (Supplemental Figure S4, D and E). The activation state of Src2 was determined as the ratio between autophosphorylation and total Src2 signal in two independent experiments (Supplemental Figure S4E), and it was not affected by the presence of the EGFP-tag for all constructs, including wild-type, membrane localization-deficient (G2A), kinase dead (K286M), and constitutively active (Y518F) Src2. Both the membrane localization-deficient and kinase dead mutants had significantly reduced activation states compared with wild type Src2. The fact that wild type and constitutively active Src2 have a similar activation state when expressed in Sf9 and SYF (data not shown) cells is most likely due to the insignificant recognition and phosphorylation of the *Aplysia* Src2 C terminus by the C-terminal Src kinase Csk expressed in the insect cells and mouse fibroblasts, respectively. Indeed, the highly conserved Glu (Y-3 position) and Gln (Y-1 position), which are critical for tail phosphorylation in vertebrates (Wang *et al*., 2001), are both different in *Aplysia* Src2. Finally, the morphology of growth cones expressing wild-type or constitutively active Src2 was independent of the presence of the EGFP-tag (Figure 8). Thus, from these results we conclude that the C-terminal EGFP-tag does not interfere with the activation or negative tail regulation of Src2.

To express proteins in cultured *Aplysia* bag cell neurons, we developed an mRNA microinjection method that is similar to the method reported recently (Sahly *et al*., 2003). In vitro transcribed mRNAs encoding Src-EGFP fusion proteins were microinjected into the cytoplasm of neuronal cell bodies together with 3-kDa-Texas Red-dextran, an injection and volume marker. Expression of EGFP-fusion proteins was typically assessed 18–20 h after microinjection (Figure 3). EGFP exhibited a volume-dependent distribution in growth cones like dextran (Figure 3, A–D), with higher signals in the C domain and the ruffling T zone (arrow in Figure 3D) than in the flatter P domain. The overlay of the EGFP and dextran images (Figure 3D) showed a strong overlap of the two probes that correlated well with the growth cone structure in the differential interference contrast (DIC) image (Figure 3A).

In contrast, both Src1- and Src2-EGFP showed a homogenous distribution in the P domain and T zone (Figure 3, E–L) that was very different from the EGFP and dextran distribution, suggesting a plasma membrane localization of each of the fusion proteins. Both Src1- and Src2-EGFP signals were elevated in the C domain compared with the P domain and the T zone (Figure 3, G and K). Overlays further confirmed that both Src1- and Src2-EGFP had a distribution very different from that of dextran (Figure 3, H and L). The morphology of Src-EGFP–expressing growth cones was not significantly different from EGFP-expressing or control growth cones. To confirm plasma membrane association of Src1 and Src2, we expressed Src-G2A-EGFP mutants, which cannot be myristoylated. These G2A mutants showed a volume-dependent distribution reminiscent of cytosolic proteins (Figure 3, M–T). Finally, FRAP analysis of the lateral mobility of Src1- and Src2-EGFP in the growth cone P domain revealed diffusion constants typical for lipid-modified signaling proteins associated with the plasma membrane (Supplemental Figure S5). Assuming purely lateral diffusion, we determined a diffusion constant of $D = 0.48 \pm 0.03\ \mu m^2/s$ for Src1-EGFP (Supplemental Figure S5, A and C) and $D = 0.38 \pm 0.03\ \mu m^2/s$ for Src2-EGFP (Supplemental Figure S5, B and D), which are slightly lower than the value of $D = 0.57\ \mu m^2/s$ that has been recently reported for chicken Src-EGFP expressed in COS-7 cells (Shvartsman *et al*., 2007). In summary, our live cell imaging data indicate that both Src1- and Src2-EGFP are localized largely to the plasma membrane of growth cones and that this membrane association likely requires N-terminal myristoylation.

Dynamics of Src2-positive Puncta and Tubular Structures

Time-lapse movies of Src-EGFP–expressing growth cones revealed homogeneous plasma membrane-associated Src-EGFP signals with intensity fluctuations (Supplemental Videos 1–3 and 6) that could reflect Src mobility in the plasma membrane because Src exhibits lateral diffusion (Supplemental Figure S5). In addition, we also observed more intense Src1- and Src2-positive puncta (typically $<1\ \mu m$ in diameter) moving in a linear manner and bidirectionally in all three growth cone domains. We focused our quantitative analysis on the movements of Src2-EGFP–positive structures. Figure 4, A and B, show a Src2-EGFP–expressing growth cone with puncta moving in a linear manner both anterogradely and retrogradely in the T zone and P domain (Supplemental Videos 1 and 2). Some puncta changed their shape over time (Figure 4B, red box), whereas others did not (Figure 4B, yellow box). We also observed many Src2-EGFP–positive puncta undergoing bidirectional movement in the C domain and analyzed those puncta that we could clearly follow over time (Figure 4, E and F). Although the puncta in the P domain and T zone moved predominantly in retrograde direction (86% of time spent) with short stationary (8%) or anterograde (6%) phases, the C domain puncta moved relatively equally in both directions, with frequent switching of direction (40% time spent anterogradely, 35% retrogradely, 25% stationary; Figure 4I). In the P/T domain, the time-weighted average velocity was $3.1 \pm 0.3\ \mu m/min$ for retrogradely and $9.4 \pm 1.9\ \mu m/min$ for anterogradely moving puncta (mean value ± SEM; Figure 4G). Puncta movements were also observed into and out of filopodia (data not shown). In the C domain, the time-weighted average velocities of Src2-EGFP puncta movement were higher

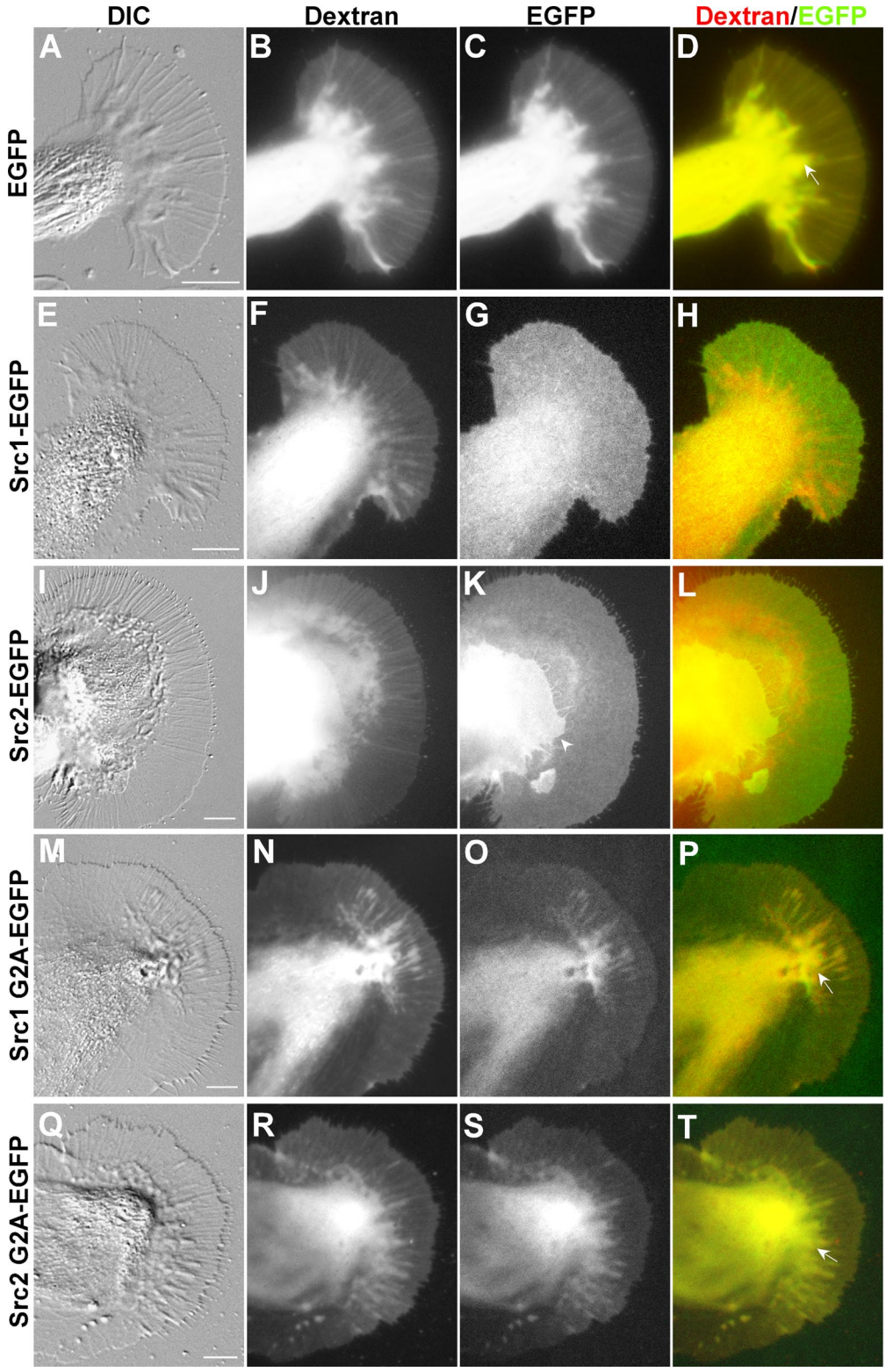

Figure 3. Src1- and Src2-EGFP localize to the plasma membrane of growth cones. Live cell fluorescence imaging of Src-EGFP fusion proteins was performed in *Aplysia* growth cones by acquiring DIC images (A, E, I, M, and Q), dextran images in the Texas Red channel (B, F, J, N, and R), and EGFP images in the FITC channel (C, G, K, O, and S). Overlays of the dextran and EGFP images are shown in (D, H, L, P, and T). (A–D) EGFP and dextran show a volume-dependent distribution in all growth cone domains. The arrow marks a T zone ruffle (D). (E–H) Src1-EGFP and (I–L) Src2-EGFP distribution indicate plasma membrane association. The white arrowhead in K marks the P domain of a second growth cone growing on top of the large growth cone, resulting in an even Src2 signal at higher intensity. Src1 G2A-EGFP (M–P) and Src2 G2A-EGFP (Q–T) exhibit a volume-dependent distribution. The arrows in P and T point toward T zone ruffles that exhibit higher signals than adjacent P domain areas. Absolute signal intensities of these G2A mutants were clearly lower compared with EGFP signals. Bars, 10 μm.

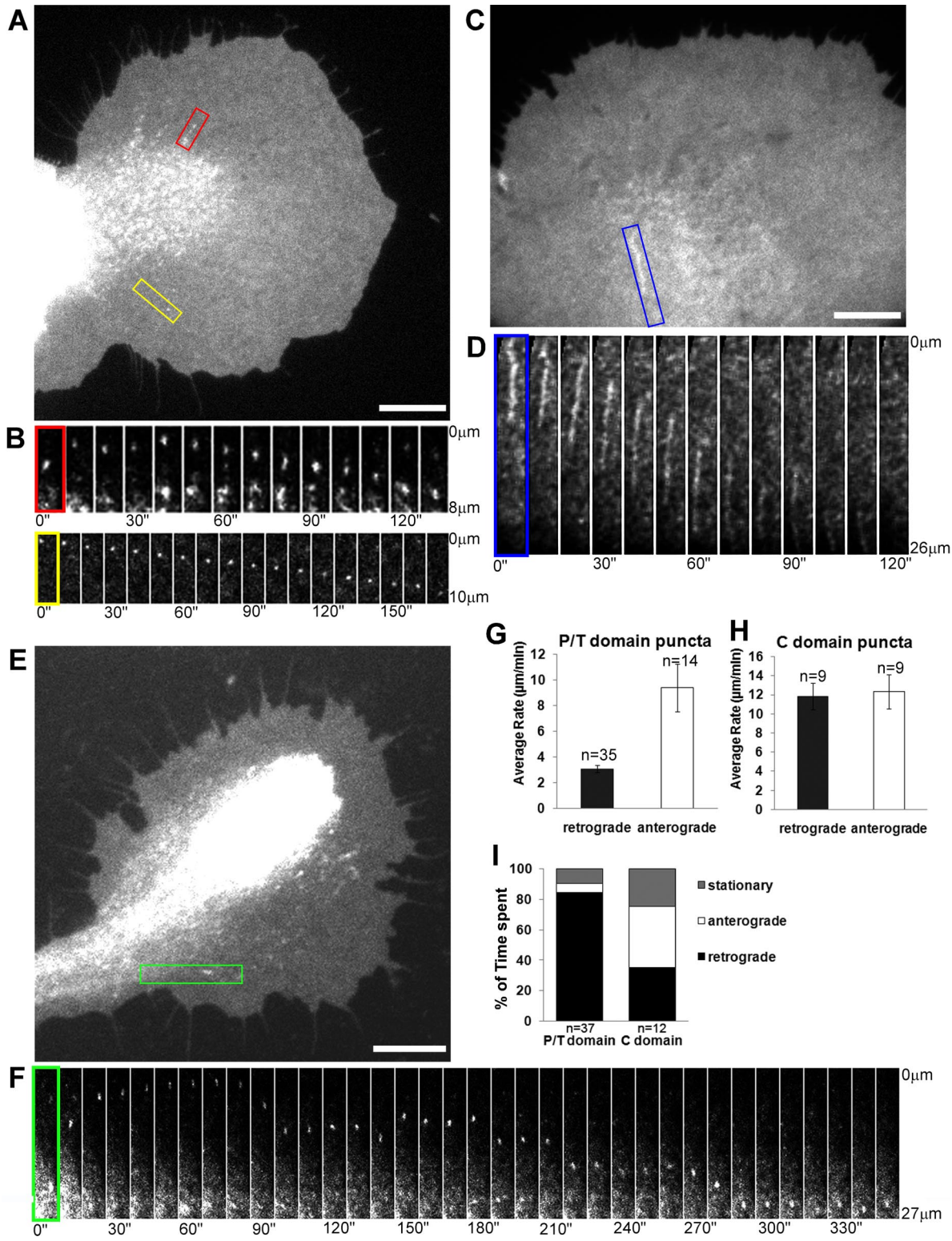

Figure 4. Dynamics of Src2-EGFP-positive puncta and tubulovesicular structures. (A) Src2-EGFP-positive puncta move in the T zone (red box; Supplemental Video 1) and in the P domain (yellow box; Supplemental Video 2). (B) Time-lapse montage of the two puncta marked in A. (C) Tubulovesicular Src2-EGFP–positive structure in the C domain (Supplemental Video 3). (D) Time-lapse montage showing the retrograde movement of the tubulovesicular structure in the region marked with a blue box in C. (E) Src2-EGFP-positive punctum moving in the C domain (green box). (F) Time-lapse montage of the C domain punctum marked in E moving bidirectionally. All intervals are 10 s. (G) Time-weighted average ± SEM rates of puncta movements in the P/T domain. (H) Time-weighted average ± SEM rates of puncta movements in the C domain. (I) Quantification of time spent by puncta moving anterogradely, retrogradely, or being stationary (n, puncta). Bars, 10 μm (A, C, and E).

than in the P/T domain: 11.8 ± 1.4 μm/min (retrograde); 12.3 ± 1.8 μm/min (anterograde) (Figure 4H). Furthermore, we frequently observed Src2-EGFP–positive elongated tubulovesicular structures (~10 μm in length) in the C domain moving mainly retrogradely in a linear manner with an average velocity of 19.0 ± 3.4 μm/min (n = 8; blue box in Figure 4, C and D; and Supplemental Videos 3 and 6).

Src2-EGFP-positive Structures Are Endocytic Vesicles Moving on Microtubules

Our movement analysis suggests that Src2-EGFP–positive puncta and tubulovesicular structures in the C domain might be Src-containing organelles moving along cytoskeletal filaments, potentially via motor-driven transport mechanisms. The lower velocity of retrogradely moving Src puncta in the P domain, in contrast, is reminiscent of F-actin- and MT-translocation rates. Thus, the puncta movements in the P domain could be due to organelles physically linked to but not moving along cytoskeletal filaments. To test whether these Src-positive internal structures are endocytic vesicles, we performed both fluid phase and plasma membrane uptake experiments by using Texas Red-dextran (70 kDa) and the lipophilic dye FM4-64, respectively (Figure 5, A–F). In the P/T domains, 60% of the Src2-EGFP–positive puncta colocalized with dextran-containing endocytic vesicles (Figure 5, A and B; n = 40 puncta, 13 growth cones), whereas in the C domain, 66% of Src2-puncta were dextran-positive (Figure 5, C and D; n = 115 puncta, 21 growth cones). Many of the Src2-EGFP–positive elongated tubulovesicular structures in C domain also labeled with dextran (data not shown) and FM4-64, indicating that these membrane structures were endocytosed (Figure 5, E and F).

Because the bidirectional movement of Src2-positive structures is suggestive of MT-based organelle transport, we performed dual channel MT/Src2-EGFP fluorescent speckle microscopy in live growth cones to test the hypothesis whether Src2-positive puncta move on or with MTs. Because of the high density of both fluorescent signals in the C domain, we focused our analysis of Src2-EGFP/tubulin overlays on the P domain and T zone. In five growth cones, we observed Src2-positive puncta moving retrogradely in concert with MT speckles (Figure 5, G and H, and Supplemental Videos 4 and 5). The example in Figure 5H shows a Src2-positive vesicle occurring in proximity of an MT undergoing retrograde translocation. The vesicle occurs at the 20-s time point and moves retrogradely in concert with a MT reference speckle. In summary, our results suggest that a significant fraction of the Src2-positive intracellular structures are endocytic vesicles, which move either together with or on microtubules.

Microtubule Association of Src2

Because the Src-EGFP–positive vesicular structures have properties of cytoskeleton-associated organelle dynamics, we tested whether endogenous Src kinases are associated with the cytoskeleton by using both an immunocytochemical and biochemical approach. Therefore, we labeled growth cones for Src1 or Src2 together with F-actin and MTs, respectively (Figure 6). Both Src1 and Src2 exhibit a partial colocalization with F-actin and MT structures in all three growth cone regions (Figure 6, A–D, arrows and insets). Activated Src2 puncta were detected at the tips of F-actin bundles in filopodia as well as adjacent to MTs (Figure 6, E, F, H, and I, arrows and insets). Colocalization analysis in the P domain and T zone revealed that the percentage of Src2-signal overlapping with MTs was only slightly higher than the percentage of MT area and not much different in pSrc2 (Figure 6, D, F, and J; see *Materials and Methods* for details).

The inability to observe a more significant Src2-MT colocalization may be due to the interference of plasma membrane-associated and cytoplasmic Src still present after regular fixation and saponin extraction. Furthermore, Src detection on MTs could be partially masked by certain organelles containing little Src. To better visualize Src2-MT colocalization in growth cones, we performed live cell extraction under cytoskeleton-stabilizing conditions (see *Materials and Methods*) before fixation and Src/MT labeling (Figure 6, G–I). This method has been used previously to demonstrate PKC-MT colocalization in *Aplysia* growth cones, which was clearly revealed only after live cell extraction but not after regular fixation (Nakhost *et al*., 2002). Similarly, we observed a significantly higher degree of Src2-MT colocalization after live cell extraction (Figure 6, G and H) compared with regular fixation (Figure 6, D and F). After live cell extraction, 62 ± 3% of the total Src2 and 54 ± 2% of the pSrc2 thresholded area overlapped with MTs in P domain and T zone (Figure 6J; average values ± SEM). These fractions of Src2- and pSrc2-signals were significantly higher than the corresponding percentage of MT areas (25 ± 1 and 27 ± 1%, respectively). These findings suggest that the colocalization is likely due to MT association of Src2 and not due to a coincidental overlay of the two signals.

To further investigate Src2-MT association, we prepared MT-enriched fractions from total *Aplysia* CNS lysates by using a cell fractionation protocol (Figure 6, K–M). The pellet after the third high-spin centrifugation (P3) contained only a few proteins, including one protein with a molecular weight of 55 kDa, whose levels were significantly increased when the sample was treated with 20 μM taxol (Figure 6K, lane P3T). Western blot analysis confirmed that this band was tubulin (Figure 6L). Activated Src2 was also detected in the P3 pellet by using the pSrc2 antibody (Figure 6L). Taxol treatment (P3T) caused an increase of pSrc2-signal (57%) similar to tubulin (74%) compared with the DMSO controls (P3C; Figure 6, L and M; n = 3). A corresponding decrease of both tubulin and pSrc2 signal was observed in the presence of 10 μM nocodazole (data not shown). The strong MT enrichment and the proportional distribution of tubulin and activated Src2 between the taxol (P3T) and control (P3C) conditions strongly suggest an MT association of activated Src2. In summary, live cell imaging and immunocytochemical and biochemical data show that a significant fraction of Src2 is associated with MTs in *Aplysia* growth cones and CNS tissue.

Microtubule-dependent Plasma Membrane Association of Src2

Based on the MT association and the dynamics of Src2-positive vesicles, we hypothesized that MTs are involved in regulating the steady state distribution of Src in the growth cone. To test this hypothesis, we treated cultured neurons with different MT depolymerizing drugs and quantified the amount of Src2-EGFP and endogenous Src2 in all three growth cone regions (Figure 7). Under control conditions, MTs dominate the C domain and T zone and continuously explore the P domain (Figure 7A, arrow) by assembly and coupling to retrograde F-actin flow (Schaefer *et al*., 2002; Suter *et al*., 2004). Src2-EGFP was uniformly distributed over the plasma membrane with higher intensities in the C domain and T zone than in the P domain, most likely due to Src2-associated organelles and plasma membrane ruffling. Treatment of the same cells with 0.05% DMSO for 1 h had no significant effect on growth cone morphology, or MT and

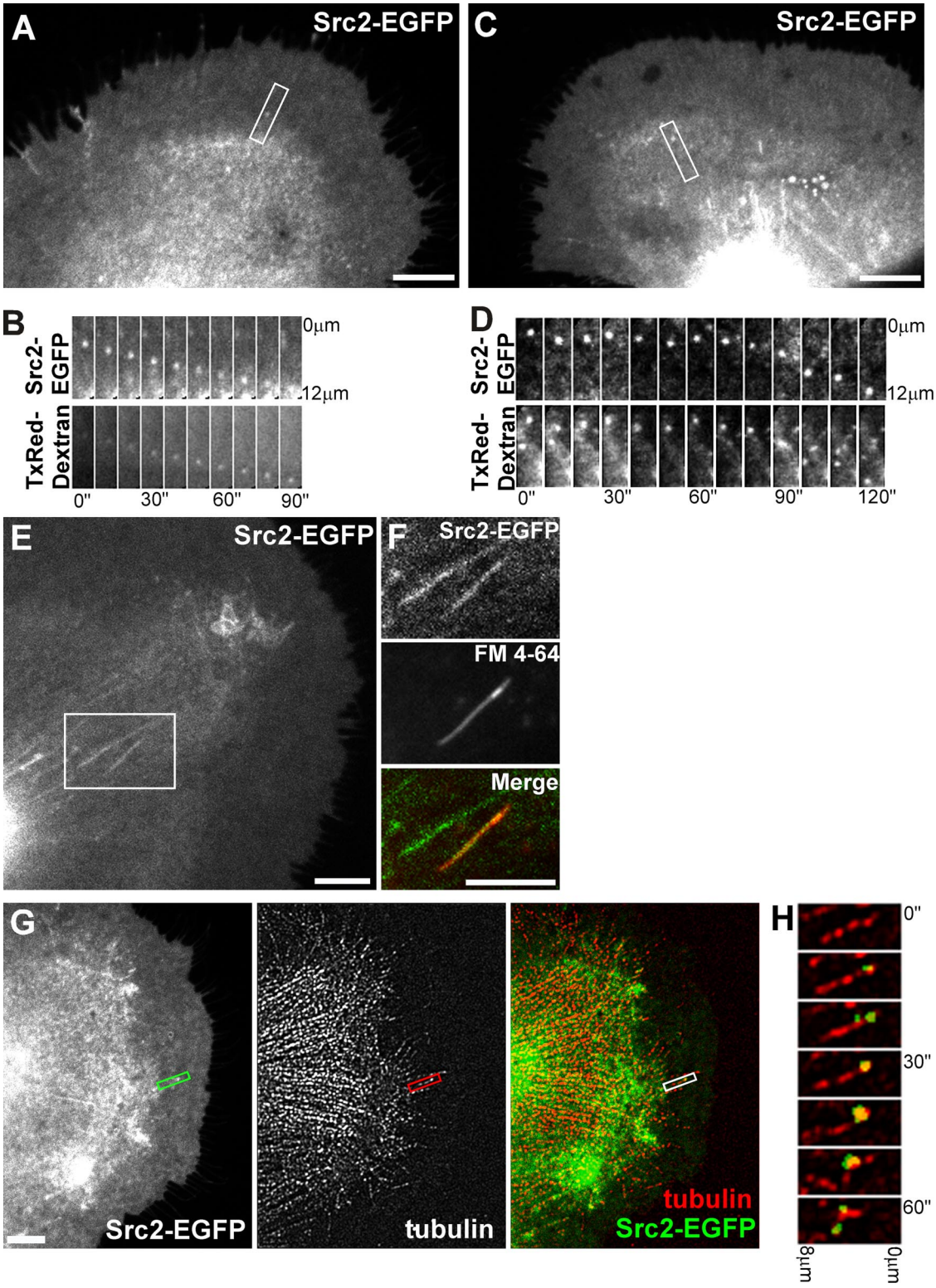

Figure 5. Src2-EGFP–positive puncta are endocytic vesicles moving with MTs. (A–D) Src2-EGFP–expressing neurons were incubated with the fluid phase uptake marker Texas Red-dextran (70 kDa). Src2-EGFP–positive puncta (marked white box) move retrogradely in the P domain (A and B) or in C domain (C and D). (B and D) Time-lapse montages (10-s intervals) show that Src2-EGFP–positive puncta contain Texas Red-dextran. (E and F) Src2-EGFP–positive tubulovesicular structures in the C domain. One of these tubular structures is also labeled with the lipophilic dye FM4-64, indicating internalized plasma membrane. (G) Src2-EGFP/tubulin FSM images of a live growth cone. Src2-EGFP channel was more processed in the overlay image than in single channel image to reveal colocalization with MT speckles. A single MT in the P domain is marked with a white box. (H) Time-lapse montage of region box-marked in H at 10-s intervals. Src2-positive punctum newly occurring in the third frame moves in concert with MT speckle for 1 min. Bars, 10 μm (A, C, E, F, and G).

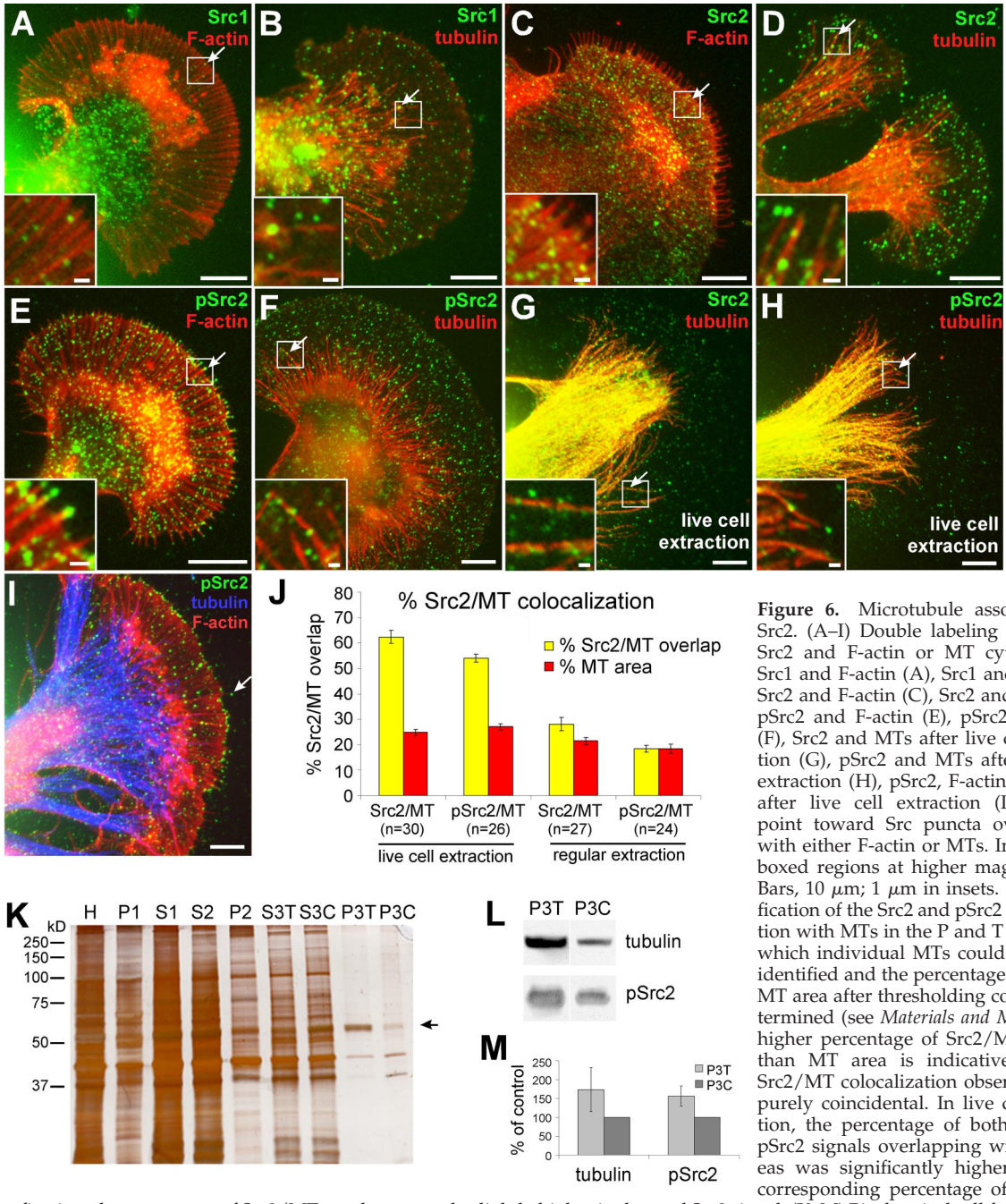

Figure 6. Microtubule association of Src2. (A–I) Double labeling of Src1 or Src2 and F-actin or MT cytoskeleton. Src1 and F-actin (A), Src1 and MTs (B), Src2 and F-actin (C), Src2 and MTs (D), pSrc2 and F-actin (E), pSrc2 and MTs (F), Src2 and MTs after live cell extraction (G), pSrc2 and MTs after live cell extraction (H), pSrc2, F-actin, and MTs after live cell extraction (I). Arrows point toward Src puncta overlapping with either F-actin or MTs. Insets show boxed regions at higher magnification. Bars, 10 μm; 1 μm in insets. (J) Quantification of the Src2 and pSrc2 colocalization with MTs in the P and T domain in which individual MTs could be clearly identified and the percentage of Src and MT area after thresholding could be determined (see *Materials and Methods*). A higher percentage of Src2/MT overlap than MT area is indicative that the Src2/MT colocalization observed is not purely coincidental. In live cell extraction, the percentage of both Src2 and pSrc2 signals overlapping with MT areas was significantly higher than the corresponding percentage of MT area. With regular fixation, the percentage of Src2/MT overlap was only slightly higher in the total Src2 signal. (K–M) Biochemical cell fractionation of *Aplysia* CNS tissue to enrich for MTs after a modified protocol originally developed by R. Vallee and G. Bloom (Vallee, 1982; Vallee and Bloom, 1983) (see *Materials and Methods* for details). (K) SDS-PAGE (10%) and silver staining of homogenate (H), high-spin pellets (P1, P2, and P3), and supernatant (S1, S2 and S3) fractions. After the 3rd centrifugation, the pellets of the taxol (P3T) and control sample (P3C) were highly enriched for microtubules. Arrow points to the 55-kDa band (tubulin), which increased in the pellet of the taxol-treated sample (P3T). (L) Western blotting of P3T and P3C fractions for tubulin and autophosphorylated Src2. pSrc2 in MT-enriched fractions proportionally increases with higher MT content in taxol-treated samples. (M) Densitometric quantification of three independent experiments. Mean values ± SEM given in percentage of DMSO control treatment.

Src2-EGFP distribution and dynamics (Figure 7B). However, additional treatment with 5 μM nocodazole for 1 h caused a small but significant increase of 12 ± 2% in P domain Src2-EGFP-levels compared with the DMSO control (Figure 7, C and F). Slightly smaller increases were observed in the T zone and C domain. As expected nocodazole treatment abolished MTs in all three growth cone domains, resulting in a diffuse tubulin signal (Figure 7C). Time-lapse imaging confirmed that MT-dependent transport of Src2-EGFP–positive vesicles and tubulovesicular structures were completely abolished after treatment with 5 μM nocodazole treatment for 1 h (Supplemental Video 6). Similar results were obtained when cells were treated with 5 μM vinblastine for 1 h (unpublished data).

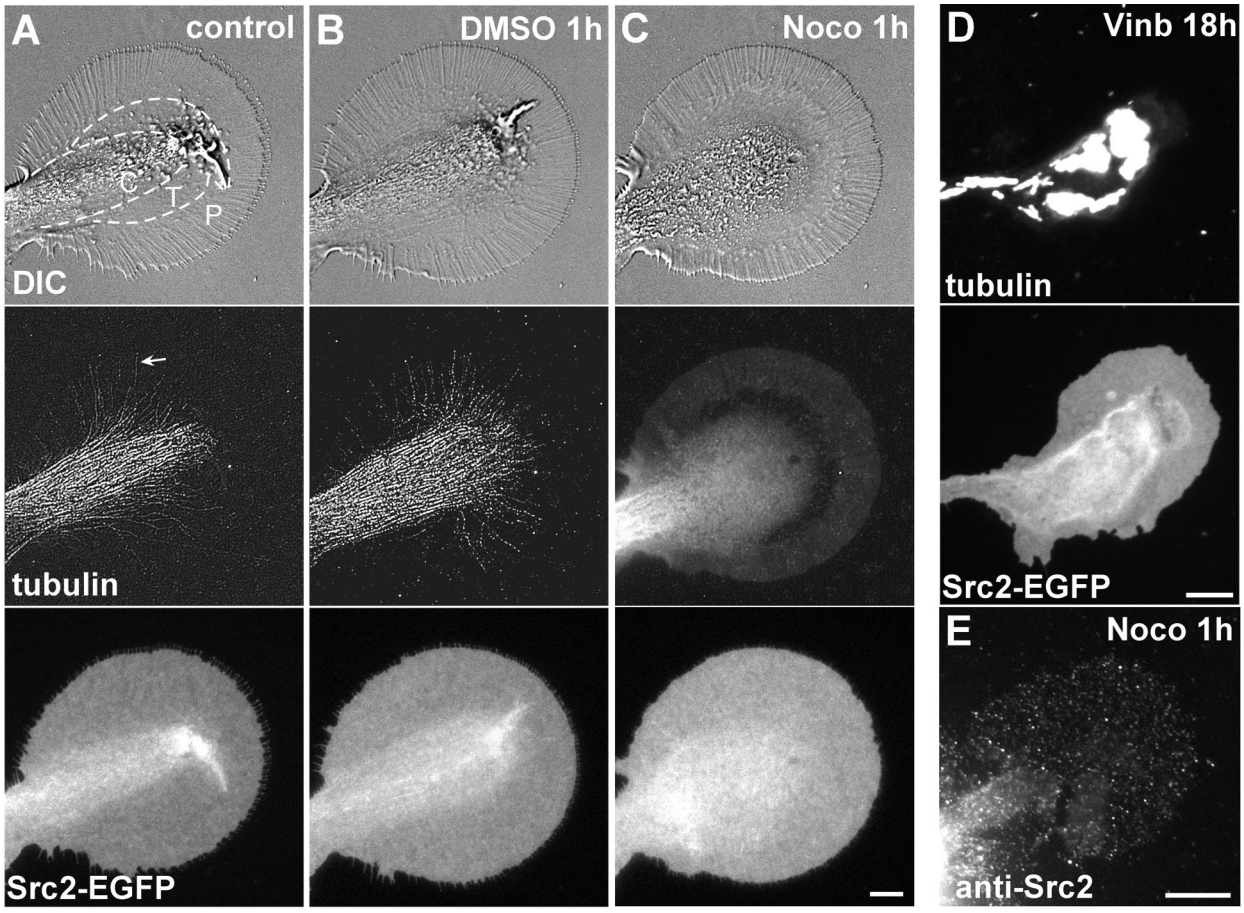

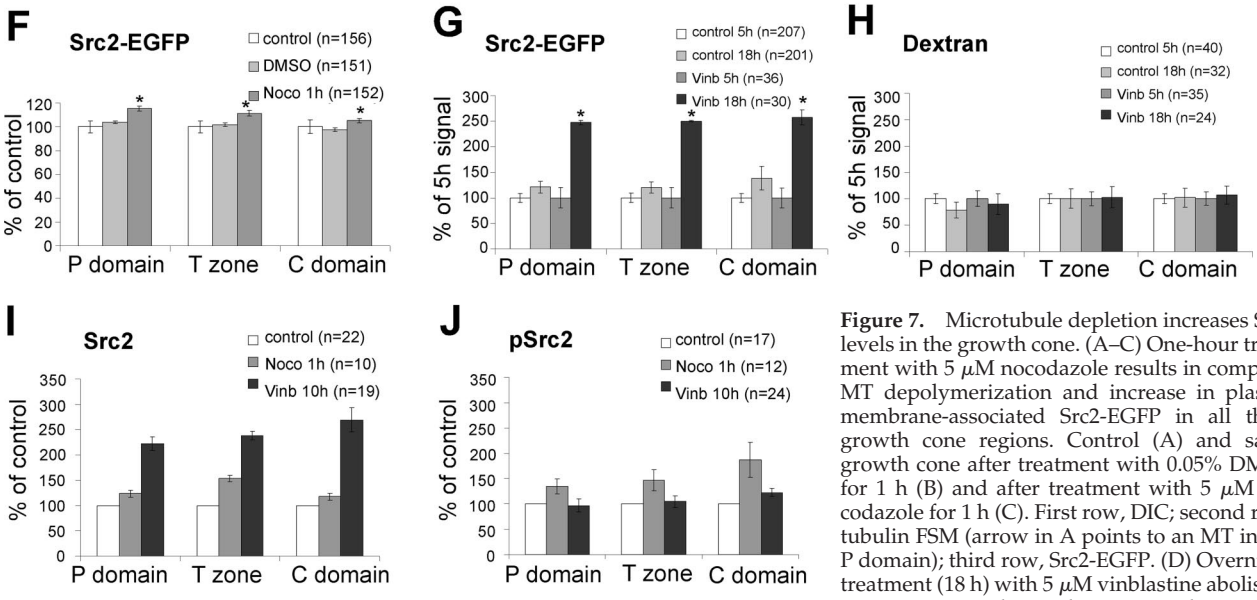

Figure 7. Microtubule depletion increases Src2 levels in the growth cone. (A–C) One-hour treatment with 5 μM nocodazole results in complete MT depolymerization and increase in plasma membrane-associated Src2-EGFP in all three growth cone regions. Control (A) and same growth cone after treatment with 0.05% DMSO for 1 h (B) and after treatment with 5 μM nocodazole for 1 h (C). First row, DIC; second row, tubulin FSM (arrow in A points to an MT in the P domain); third row, Src2-EGFP. (D) Overnight treatment (18 h) with 5 μM vinblastine abolishes MTs in axons and growth cones, resulting in MT aggregation and increased Src2-EGFP signals in all three growth cone regions. (E) Src2 immunocytochemistry of a growth cone treated with 5 μM nocodazole for 1 h. Bars, 10 μm. (F) Quantification of Src2-EGFP in 5 μM nocodazole (1-h) experiment. (G) Quantification of Src2-EGFP in long-term vinblastine experiment (18 h; 5 μM vinblastine). Percentage of intensity change relative to 5-h time point is given for both control and vinblastine cells. Asterisks in F and G indicate significant differences from control with $p < 10^{-5}$ (*t* test). (H) Texas Red-dextran volume signal does not change by long-term vinblastine treatment. (I) Endogenous Src2 levels increased in all domains after treatment with 5 μM nocodazole for 1 h or 5 μM vinblastine for 10 h, respectively. (J) Quantification of endogenous Src2 activation levels. n, number of growth cones; all experiments were carried out at least twice.

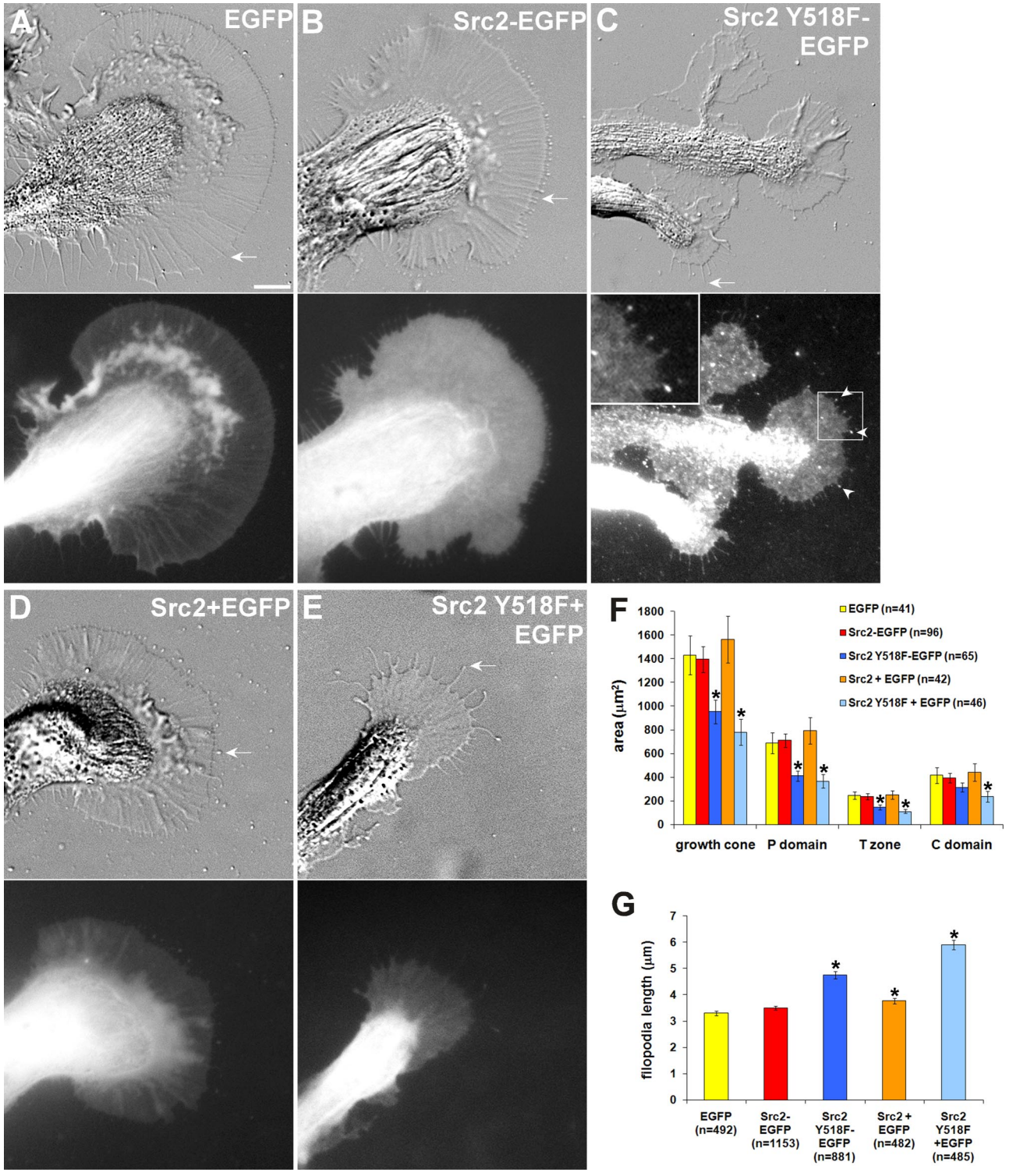

Figure 8. Src2 regulates growth cone size and filopodia length. EGFP (A), Src2-EGFP (B), Src2 Y518F-EGFP (C), Src2 + EGFP (2:1) (D), and Src2 Y518F + EGFP (2:1) (E) were expressed in neurons and imaged with both DIC (top row) and FITC filter optics (bottom row) after 20 h of expression. Overall expression levels of constitutively active Src2-mutant were lower than of wild-type Src2. Src2 Y518-EGFP signal is increased in filopodia tips (arrowhead in C). Inset in C is magnified by factor 2.5. Bar, 10 μm. Only EGFP-positive growth cones were included in the quantification. (F) Mean ± SEM values of total growth cone size as well as of the P domain, T zone, and C domain were determined from n = 40 to 100 growth cones in four independent experiments. Asterisks indicate significant differences to EGFP control size with $p < 0.05$ (t test). Constitutively active Src2 significantly reduced growth size independently of the EGFP moiety. (G) Constitutively active Src significantly increased filopodia length (average length ± SEM from n = 400 to 1200 filopodia per condition). Asterisks indicate significant difference to control filopodia with $p < 0.01$ (t test).

We also treated the cells for up to 18 h with 5 μM vinblastine. This over night vinblastine treatment abolished MT structure not only in growth cones but also in axons, resulting in the well-known vinblastine-induced tubulin aggregation (Luduena *et al*., 1984) in the C domain and axons (Figure 7D). To control for different expression levels, Src2-EGFP levels in control and drug-treated cells were monitored in parallel between 5 and 18 h of treatment (Figure 7G). Although control cells showed a 21 $\pm$ 11% increase of Src2-EGFP in the P domain between 5 and 18 h, a significantly larger increase of 147 $\pm$ 4% was measured in vinblastine-treated cells. The relative increases in the other domains were similar. We do not believe that the increased Src2 levels could be due to significant volume changes after the MT drug treatments for the following reasons: 1) the Src-EGFP signal does not show a volume-dependent distribution; and 2) the 3-kDa Texas Red-dextran volume signal was unaffected by the same MT drug treatments (Figure 7H).

Furthermore, we assessed the effects of short and long-term MT depletion on endogenous Src2 levels and activation by immunocytochemistry (Figure 7, E, I, and J). Src2 distribution remained punctate because of saponin extraction of the plasma membrane, and Src2 levels were increased in all three regions after treatment with 5 μM nocodazole for 1 h (Figure 7, E and I; 23 $\pm$ 7% increase in the P domain) and 5 μM vinblastine for 10 h (122 $\pm$ 13% increase in the P domain). Interestingly, Src2 activation signals detected by pSrc2 were also increased after 1 h of MT disruption by nocodazole, but they were at control levels after 10-h depletion by vinblastine (Figure 7J). Thus, the relative activation state of endogenous Src2 was significantly lower after the 10-h vinblastine treatment. In summary, various MT depletion protocols resulted in significant increases of both expressed Src2 and endogenous Src2, suggesting that MTs play a critical role in regulating the steady-state distribution as well as the activation state of Src2 in the growth cone plasma membrane.

Src2 Regulates Growth Cone Size and Filopodia Length

To gain insight into the function of Src2 in growth cones, we expressed wild-type Src2 and the constitutively active Src2 Y518F mutant with or without the EGFP-tag in *Aplysia* neurons, and we compared their growth cones with the ones from EGFP-expressing control neurons (Figure 8). As already shown in Figure 3, the morphology of growth cones expressing Src2-EGFP was very similar to control growth cones expressing EGFP (Figure 8, A and B). In contrast, Src2 Y518F-EGFP–expressing neurons had smaller growth cones with longer filopodia (arrows) compared with EGFP- or Src2-EGFP–expressing neurons (Figure 8C). The plasma membrane signal of constitutively active Src2 Y518F-EGFP was less uniform than that of wild-type Src2-EGFP; it was concentrated in filopodia tips (arrowhead) and relative stable punctate structures throughout the growth cone, which could be point contacts (Woo and Gomez, 2006) that were induced by expression of constitutively active Src2 (inset in Figure 8C). Interestingly, we did not observe any distinct Src2 Y518F-EGFP–positive vesicles moving in a linear manner in any of the growth cone domains as found for wild-type Src2-EGFP (Supplemental Figure S6 and Supplemental Video 7). However, Texas Red-dextran–positive vesicle movements could be detected in the growth cones expressing Src2 Y518F-EGFP, suggesting that endocytosis in general is not affected, whereas internalization of activated Src2 is reduced (Supplemental Figure S6B).

Generally, expression levels of constitutively active Src2 seemed lower than those of wild-type Src2. Similarly, growth cones expressing Src2 Y518F were smaller with longer filopodia than the ones expressing wild-type Src2 (Figure 8E; EGFP was used as an expression marker in untagged Src constructs). Both Src2 Y518F-EGFP and Src2 Y518F reduced the size of the growth cones by 33 and 45%, respectively, compared with EGFP-expressing growth cones (Figure 8F; *t* test: $p < 0.05$, asterisks). Growth cone size was not significantly different between the two constitutively active Src2 constructs. Growth cones expressing Src2-EGFP and Src2 were similar in size to growth cones expressing EGFP. Regional size analysis of the P domain, T zone and C domain revealed that constitutively active Src2 reduced the size of all growth cone domains proportionally. Filopodia in neurons expressing either Src2 Y518F-EGFP or Src2 Y518F were 42 and 77% longer, respectively, compared with EGFP controls (Figure 8G; $p < 10^{-5}$), whereas filopodia in Src2-expressing neurons were only 11% longer than filopodia of EGFP-expressing control neurons ($p < 0.01$). Thus, overexpression of either EGFP-tagged or untagged wild-type Src2 did not significantly affect the morphology of the growth cones, whereas overexpression of constitutively active Src2 decreased growth cone size and increased filopodia length, implicating a role for Src in regulating lamellipodia and filopodia size.

DISCUSSION

To investigate the distribution, trafficking, activation state, and function of Src tyrosine kinases in the growth cone, we performed high-resolution live cell imaging of two novel Src PTKs, Src1 and Src2, in cultured *Aplysia* growth cones. We found that both kinases are associated with the plasma membrane, partially colocalize with the cytoskeleton and undergo vesicular MT-dependent movements upon endocytosis. Our results suggest that MTs control the steady state distribution and activation state of Src2, which could be important for growth cone responses to guidance cues.

Live Cell Imaging of Src in Growth Cones

Because Src undergoes conformational changes during activation/inactivation (Boggon and Eck, 2004), it is crucial to test whether localization and activation state of the fusion protein is affected by the GFP-tag (Sandilands *et al*., 2004). Molecular modeling, biochemical data, and phenotype analysis suggest that our Src-EGFP fusion construct faithfully reflects the molecular actions of endogenous Src in the growth cone. In addition, our construct was designed almost identically to the construct used by Sandilands and colleagues, which had normal activity and tail regulation (Sandilands *et al*., 2004). Live cell imaging of Src1- and Src2-EGFP revealed that a significant fraction of Src is localized to the growth cone plasma membrane where it exhibits lateral diffusion (Figure 3 and Supplemental Figure S5). In addition, both Src PTKs are associated with organelles of the endocytic machinery and the cytoskeleton (Figures 4–6), which is in agreement with earlier biochemical studies on growth cone particles (Maness *et al*., 1988; Bixby and Jhabvala, 1993; Helmke and Pfenninger, 1995). In nonneuronal cells, a significant fraction of Src PTKs is associated with the plasma membrane and endosomes (Courtneidge *et al*., 1980; Kaplan *et al*., 1992; Alland *et al*., 1994; Sandilands *et al*., 2004; Kasahara *et al*., 2007b). Plasma membrane association of Src PTKs is mediated by myristoylation of the conserved glycine 2, additional palmitoylation of cysteine, the presence of lysine residues in the N terminus as well as additional sequences in the unique region of the N-terminus that allow interactions with different receptor proteins (Silverman and Resh, 1992;

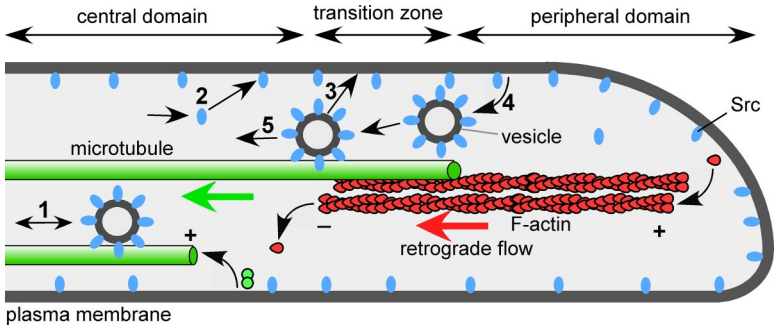

Figure 9. Model of Src trafficking in the growth cone. Schematic depicting a cross-section through the three regions of a growth cone and various steps of Src trafficking. Bidirectional MT-based organelle transport in the C domain suggests that Src is delivered on vesicles from the axon into the growth cone as well as retrogradely out of the growth cone (1). A portion of Src could enter the growth cone also by diffusion through the cytoplasm (2). Organelle-mediated delivery could result in Src association with the plasma membrane in the growth cone (3). The relative proportions of cytoplasmic diffusion, organelle-mediated delivery on either microtubules or F-actin (not depicted) as well as of local Src translation (not shown) are not known. Src is retrieved from the plasma membrane by endocytosis in the P domain and T zone (4). Src-positive vesicles undergo retrograde movements in association with MTs. Our data provide evidence for steps 1, 4, and 5 in this model (5).

Alland *et al*., 1994; Thomas and Brugge, 1997). Because the G2A mutation largely abolished plasma membrane localization of both Src1 and Src2 (Figure 3), we conclude that myristoylation is essential for plasma membrane association of both kinases in growth cones. The G2A mutant also had reduced activation levels (Supplemental Figure S4); thus, a significant portion of Src activation occurs at the plasma membrane, which is in agreement with the localization of activated Src2 and constitutively active Src2 at tips of filopodia. In addition, activated Src is also associated with the MT and F-actin cytoskeleton. Thus, we propose that Src activation in growth cones can happen both at the plasma membrane and on cytoskeletal structures, which is consistent with findings in nonneuronal cells (Sandilands *et al*., 2004).

Src2 Levels in the Growth Cone Are Controlled by Microtubules

Biochemical and imaging data provide evidence for MT association of Src2 in growth cones. The movement of Src2-positive vesicles in the C domain was bidirectional, whereas it was predominantly retrograde in the P/T domains. In the P/T domains, 60% of the Src2-positive vesicles were dextran positive, suggesting that the Src2-labeled vesicles had been internalized from the plasma membrane, whereas the residual 40% could have been endocytosed after dextran washout. Dual-channel FSM revealed that in the P domain, a fraction of Src2-positive vesicles move retrogradely either together with or on microtubules. The faster moving tubular structures in the C domain are likely tubulovesicular recycling endosomes that are transported by motor proteins along MTs (Prekeris *et al*., 1999). Our findings on Src association with MTs are consistent with previous studies in both nonneuronal cells (Abu-Amer *et al*., 1997; Yamada *et al*., 2000) and neurons (Matten *et al*., 1990; Helmke and Pfenninger, 1995; Lee, 2005); however, the dynamic relationship between Src and MTs has not been studied so far. Additional actin imaging and perturbation studies are needed to investigate whether F-actin plays a role in Src turnover in growth cones as well.

How could Src bind to MTs in growth cones? Individual Src molecules could bind to MTs either directly or indirectly via MT-associated proteins tau and MAP2 (Matten *et al*., 1990; Lee *et al*., 1998; Lim and Halpain, 2000). The Src-EGFP puncta observed in the present study, however, likely reflect vesicle-associated Src based on their size (<1 μm), movement characteristics, and labeling with endocytic markers. Although MT-dependent Src association with endosomal membranes has been demonstrated in fibroblasts (Kaplan *et al*., 1992), surprisingly little is known about intracellular Src trafficking in general. Do Src PTKs move by organelle-mediated trafficking or cytosolic diffusion between the Golgi complex and the plasma membrane? In nonneuronal cells evidence has been provided for both mechanisms: vesicular transport (Bijlmakers and Marsh, 1999; Kasahara *et al*., 2004; Sandilands *et al*., 2004) and diffusion through the cytosol (Kasahara *et al*., 2007a).

In growth cones, however, Src trafficking has not been studied to date. Our data suggest a dynamic association of Src with MTs and a role for MTs in Src turnover in growth cones (Figure 9). How could Src be delivered into the growth cone? The anterograde transport of vesicle-associated Src2 in the C domain suggests that MTs can act as tracks for Src delivery from the axon into the growth cone (Figure 9, step 1). Diffusion of cytoplasmic Src (step 2), actin-based transport, and local translation in the growth cone (not depicted in Figure 9) could also increase the amounts of Src. Within the growth cone, Src could get to the plasma membrane either by diffusion (step 2) or vesicle-mediated delivery (step 3). To maintain a steady-state Src2 level at the plasma membrane, Src2 undergoes endocytosis (step 4), retrograde MT-based transport with endocytic vesicles (step 5) and perhaps recycling back to the plasma membrane (step 3). When growth cones were depleted from MTs, we observed a significant increase in Src2 levels in all domains, supporting that the idea that the net direction of MT-based Src trafficking in growth cones is retrograde. Besides supporting retrograde transport of endocytosed Src2, MTs could also mediate the actual Src2 internalization process itself (step 4), because MTs have been implicated in the internalization of the transferrin receptor in nonneuronal cells (Jin and Snider, 1993; Subtil and Dautry-Varsat, 1997). Last, we can also not exclude the possibility that MTs play a role in Src2 degradation in the growth cone.

In summary, our data suggest that MTs play a key role in regulating the steady-state levels and turnover of Src in the growth cone by at least two mechanisms: by transporting Src bidirectionally in the C domain (Figure 9, step 1) and by retrogradely transporting Src2-positive vesicles that have been internalized by endocytosis in the P domain and T zone (Figure 9, step 5). In addition, our results indicate that MTs also regulate the activation state of Src2 at the plasma membrane, for example via MT-dependent delivery of Src activators. This is consistent with a role of dynamic microtubules in Src activation at adhesion sites (Suter *et al*., 2004).

Src2 Activation Affects Growth Cone Morphology

How Src activity regulates growth cone morphology and motility is largely unknown. Active endogenous Src2 accumulates in the tips of filopodia of *Aplysia* growth cones,

which is consistent with recent findings in *Xenopus* growth cones (Robles *et al*., 2005). Furthermore, constitutively active Src2-EGFP is concentrated in filopodia tips of *Aplysia* growth cones and induces smaller growth cones with longer filopodia when compared with growth cones expressing EGFP or wild type Src2-EGFP (Figure 8). Such a phenotype could be favorable for faster growth and improved detection of guidance information. That the wild-type Src2 expression did not significantly alter growth cone morphology indicates that Src activation is tightly controlled in growth cones.

Interestingly, constitutively active Src2 undergoes less recycling compared with wild-type Src2. We did not observe Src2 Y518F-EGFP–positive vesicles moving in the growth cone, whereas movements of dextran-positive vesicles seemed to be unaffected, suggesting that endocytosis of active Src2 but not dextran is reduced. Thus, constitutively active Src2 at the plasma membrane is more stable compared with wild-type Src2. These observations are consistent with the slower FRAP recovery rates of active Src as well as with the localization of active Src to focal adhesions in nonneuronal cells (Kasahara *et al*., 2007a; Shvartsman *et al*., 2007). To which extent the increased membrane stability of constitutively active Src2 contributes to the observed growth cone phenotype is unclear. The length of filopodia is largely determined by F-actin dynamics, and it has been shown that Src-dependent tyrosine phosphorylation at filopodia tips can regulate filopodial dynamics and initiation (Robles *et al*., 2005). The reduced growth cone size induced by constitutively active Src2 could be due to alterations in both F-actin and MT structure and dynamics, for example through Rho GTPases. Future studies using various Src2 mutants in combination with quantitative analysis of cytoskeletal dynamics will provide more detailed insights into the mechanisms of how Src affects growth cone motility and guidance. Furthermore, because Src activation has been implicated in cell adhesion-cytoskeletal coupling and related growth cone steering (Suter *et al*., 2004), it will be interesting to test whether Src2 is recruited to adhesion sites or just locally activated.

ACKNOWLEDGMENTS

We thank Dr. Nelson Medeiros (Yale University, New Haven, CT) and Doris Kemler for initial assistance with PCR cloning, and Drs. Steve Goldstein (Yale University) and Wayne Sossin (McGill University, Montreal, QC, Canada) for providing vectors. We are grateful to Dr. Carol Post for assistance with molecular modeling and to Dr. Jennifer Hovis for discussion of FRAP data. We thank Lauren Sanchez for help with immunostainings; Aih Cheun Lee for assistance with Src2-trafficking experiments; and Drs. Robert Geahlen, Peter Hollenbeck and Don Ready as well as members of the Suter laboratory for valuable comments on the manuscript.

This work was supported by National Institutes of Health grant R01 NS-049233 and a grant from the Bindley Bioscience Center at Purdue University (to D.M.S.). Research contributions by M. Z. and W. K. were supported by Summer Research Internships sponsored by the Howard Hughes Medical Institute.

REFERENCES

Abu-Amer, Y., Ross, F. P., Schlesinger, P., Tondravi, M. M., and Teitelbaum, S. L. (1997). Substrate recognition by osteoclast precursors induces C-src/microtubule association. J. Cell Biol. *137*, 247–258.

Alland, L., Peseckis, S. M., Atherton, R. E., Berthiaume, L., and Resh, M. D. (1994). Dual myristylation and palmitylation of Src family member p59fyn affects subcellular localization. J. Biol. Chem. *269*, 16701–16705.

Beggs, H. E., Soriano, P., and Maness, P. F. (1994). NCAM-dependent neurite outgrowth is inhibited in neurons from Fyn-minus mice. J. Cell Biol. *127*, 825–833.

Bijlmakers, M. J., and Marsh, M. (1999). Trafficking of an acylated cytosolic protein: newly synthesized p56(lck) travels to the plasma membrane via the exocytic pathway. J. Cell Biol. *145*, 457–468.

Bixby, J. L., and Jhabvala, P. (1993). Tyrosine phosphorylation in early embryonic growth cones. J. Neurosci. *13*, 3421–3432.

Boggon, T. J., and Eck, M. J. (2004). Structure and regulation of Src family kinases. Oncogene *23*, 7918–7927.

Brown, M. T., and Cooper, J. A. (1996). Regulation, substrates and functions of src. Biochim. Biophys. Acta *1287*, 121–149.

Burden-Gulley, S. M., and Lemmon, V. (1996). L1, N-cadherin, and laminin induce distinct distribution patterns of cytoskeletal elements in growth cones. Cell Motil. Cytoskeleton *35*, 1–23.

Carreno, S., Gouze, M. E., Schaak, S., Emorine, L. J., and Maridonneau-Parini, I. (2000). Lack of palmitoylation redirects p59Hck from the plasma membrane to p61Hck-positive lysosomes. J. Biol. Chem. *275*, 36223–36229.

Courtneidge, S. A., Levinson, A. D., and Bishop, J. M. (1980). The protein encoded by the transforming gene of avian sarcoma virus (pp60src) and a homologous protein in normal cells (pp60proto-src) are associated with the plasma membrane. Proc. Natl. Acad. Sci. USA *77*, 3783–3787.

Cross, F. R., Garber, E. A., Pellman, D., and Hanafusa, H. (1984). A short sequence in the p60src N terminus is required for p60src myristylation and membrane association and for cell transformation. Mol. Cell Biol. *4*, 1834–1842.

Falk, J., *et al*. (2005). Dual functional activity of semaphorin 3B is required for positioning the anterior commissure. Neuron *48*, 63–75.

Fessart, D., Simaan, M., Zimmerman, B., Comeau, J., Hamdan, F. F., Wiseman, P. W., Bouvier, M., and Laporte, S. A. (2007). Src-dependent phosphorylation of beta2-adaptin dissociates the beta-arrestin-AP-2 complex. J. Cell Sci. *120*, 1723–1732.

Forscher, P., Kaczmarek, L. K., Buchanan, J. A., and Smith, S. J. (1987). Cyclic AMP induces changes in distribution and transport of organelles within growth cones of *Aplysia* bag cell neurons. J. Neurosci. *7*, 3600–3611.

Gasman, S., Kalaidzidis, Y., and Zerial, M. (2003). RhoD regulates endosome dynamics through Diaphanous-related Formin and Src tyrosine kinase. Nat. Cell Biol. *5*, 195–204.

Grant, S. G., O'Dell, T. J., Karl, K. A., Stein, P. L., Soriano, P., and Kandel, E. R. (1992). Impaired long-term potentiation, spatial learning, and hippocampal development in fyn mutant mice. Science *258*, 1903–1910.

Helmke, S., and Pfenninger, K. H. (1995). Growth cone enrichment and cytoskeletal association of non-receptor tyrosine kinases. Cell Motil. Cytoskeleton *30*, 194–207.

Hoffman-Kim, D., Kerner, J. A., Chen, A., Xu, A., Wang, T. F., and Jay, D. G. (2002). pp60(c-src) is a negative regulator of laminin-1-mediated neurite outgrowth in chick sensory neurons. Mol. Cell. Neurosci. *21*, 81–93.

Ignelzi, M. A., Jr., Miller, D. R., Soriano, P., and Maness, P. F. (1994). Impaired neurite outgrowth of src-minus cerebellar neurons on the cell adhesion molecule L1. Neuron *12*, 873–884.

Jin, M., and Snider, M. D. (1993). Role of microtubules in transferrin receptor transport from the cell surface to endosomes and the Golgi complex. J. Biol. Chem. *268*, 18390–18397.

Kaplan, K. B., Swedlow, J. R., Varmus, H. E., and Morgan, D. O. (1992). Association of p60c-src with endosomal membranes in mammalian fibroblasts. J. Cell Biol. *118*, 321–333.

Kasahara, K., Nakayama, Y., Ikeda, K., Fukushima, Y., Matsuda, D., Horimoto, S., and Yamaguchi, N. (2004). Trafficking of Lyn through the Golgi caveolin involves the charged residues on alphaE and alphaI helices in the kinase domain. J. Cell Biol. *165*, 641–652.

Kasahara, K., Nakayama, Y., Kihara, A., Matsuda, D., Ikeda, K., Kuga, T., Fukumoto, Y., Igarashi, Y., and Yamaguchi, N. (2007a). Rapid trafficking of c-Src, a non-palmitoylated Src-family kinase, between the plasma membrane and late endosomes/lysosomes. Exp. Cell Res. *313*, 2651–2666.

Kasahara, K., Nakayama, Y., Sato, I., Ikeda, K., Hoshino, M., Endo, T., and Yamaguchi, N. (2007b). Role of Src-family kinases in formation and trafficking of macropinosomes. J. Cell Physiol. *211*, 220–232.

Knoll, B., and Drescher, U. (2004). Src family kinases are involved in EphA receptor-mediated retinal axon guidance. J. Neurosci. *24*, 6248–6257.

Lee, G. (2005). Tau and src family tyrosine kinases. Biochim. Biophys. Acta *1739*, 323–330.

Lee, G., Newman, S. T., Gard, D. L., Band, H., and Panchamoorthy, G. (1998). Tau interacts with src-family non-receptor tyrosine kinases. J. Cell Sci. *111*, 3167–3177.

Li, W., *et al*. (2004). Activation of FAK and Src are receptor-proximal events required for netrin signaling. Nat. Neurosci. *7*, 1213–1221.

Lim, R. W., and Halpain, S. (2000). Regulated association of microtubule-associated protein 2 (MAP2) with Src and Grb *2*, evidence for MAP2 as a scaffolding protein. J. Biol. Chem. *275*, 20578–20587.

Liu, G., Beggs, H., Jurgensen, C., Park, H. T., Tang, H., Gorski, J., Jones, K. R., Reichardt, L. F., Wu, J., and Rao, Y. (2004). Netrin requires focal adhesion kinase and Src family kinases for axon outgrowth and attraction. Nat. Neurosci. *7*, 1222–1232.

Luduena, R. F., Fellous, A., McManus, L., Jordan, M. A., and Nunez, J. (1984). Contrasting roles of tau and microtubule-associated protein 2 in the vinblastine-induced aggregation of brain tubulin. J. Biol. Chem. *259*, 12890–12898.

Maness, P. F., Aubry, M., Shores, C. G., Frame, L., and Pfenninger, K. H. (1988). c-src gene product in developing rat brain is enriched in nerve growth cone membranes. Proc. Natl. Acad. Sci. USA *85*, 5001–5005.

Maness, P. F., Beggs, H. E., Klinz, S. G., and Morse, W. R. (1996). Selective neural cell adhesion molecule signaling by Src family tyrosine kinases and tyrosine phosphatases. Perspect. Dev. Neurobiol. *4*, 169–181.

Matten, W. T., Aubry, M., West, J., and Maness, P. F. (1990). Tubulin is phosphorylated at tyrosine by pp60c-src in nerve growth cone membranes. J. Cell Biol. *111*, 1959–1970.

Meriane, M., Tcherkezian, J., Webber, C. A., Danek, E. I., Triki, I., McFarlane, S., Bloch-Gallego, E., and Lamarche-Vane, N. (2004). Phosphorylation of DCC by Fyn mediates Netrin-1 signaling in growth cone guidance. J. Cell Biol. *167*, 687–698.

Mettlen, M., Platek, A., Van Der Smissen, P., Carpentier, S., Amyere, M., Lanzetti, L., de Diesbach, P., Tyteca, D., and Courtoy, P. J. (2006). Src triggers circular ruffling and macropinocytosis at the apical surface of polarized MDCK cells. Traffic *7*, 589–603.

Mohamed, A. S., Rivas-Plata, K. A., Kraas, J. R., Saleh, S. M., and Swope, S. L. (2001). Src-class kinases act within the agrin/MuSK pathway to regulate acetylcholine receptor phosphorylation, cytoskeletal anchoring, and clustering. J. Neurosci. *21*, 3806–3818.

Morse, W. R., Whitesides, J. G., 3rd, LaMantia, A. S., and Maness, P. F. (1998). p59fyn and pp60c-src modulate axonal guidance in the developing mouse olfactory pathway. J. Neurobiol. *36*, 53–63.

Nakhost, A., Kabir, N., Forscher, P., and Sossin, W. S. (2002). Protein kinase C isoforms are translocated to microtubules in neurons. J. Biol. Chem. *277*, 40633–40639.

Newsome, T. P., Weisswange, I., Frischknecht, F., and Way, M. (2006). Abl collaborates with Src family kinases to stimulate actin-based motility of vaccinia virus. Cell Microbiol. *8*, 233–241.

Prekeris, R., Foletti, D. L., and Scheller, R. H. (1999). Dynamics of tubulovesicular recycling endosomes in hippocampal neurons. J. Neurosci. *19*, 10324–10337.

Robles, E., Woo, S., and Gomez, T. M. (2005). Src-dependent tyrosine phosphorylation at the tips of growth cone filopodia promotes extension. J. Neurosci. *25*, 7669–7681.

Sadasivam, G., Willmann, R., Lin, S., Erb-Vogtli, S., Kong, X. C., Ruegg, M. A., and Fuhrer, C. (2005). Src-family kinases stabilize the neuromuscular synapse in vivo via protein interactions, phosphorylation, and cytoskeletal linkage of acetylcholine receptors. J. Neurosci. *25*, 10479–10493.

Sahly, I., Erez, H., Khoutorsky, A., Shapira, E., and Spira, M. E. (2003). Effective expression of the green fluorescent fusion proteins in cultured *Aplysia* neurons. J. Neurosci. Methods *126*, 111–117.

Sandilands, E., Cans, C., Fincham, V. J., Brunton, V. G., Mellor, H., Prendergast, G. C., Norman, J. C., Superti-Furga, G., and Frame, M. C. (2004). RhoB and actin polymerization coordinate Src activation with endosome-mediated delivery to the membrane. Dev. Cell *7*, 855–869.

Schaefer, A. W., Kabir, N., and Forscher, P. (2002). Filopodia and actin arcs guide the assembly and transport of two populations of microtubules with unique dynamic parameters in neuronal growth cones. J. Cell Biol. *158*, 139–152.

Schmid, R. S., Pruitt, W. M., and Maness, P. F. (2000). A MAP kinase-signaling pathway mediates neurite outgrowth on L1 and requires Src-dependent endocytosis. J. Neurosci. *20*, 4177–4188.

Shvartsman, D. E., Donaldson, J. C., Diaz, B., Gutman, O., Martin, G. S., and Henis, Y. I. (2007). Src kinase activity and SH2 domain regulate the dynamics of Src association with lipid and protein targets. J. Cell Biol. *178*, 675–686.

Silverman, L., and Resh, M. D. (1992). Lysine residues form an integral component of a novel NH2-terminal membrane targeting motif for myristylated pp60v-src. J. Cell Biol. *119*, 415–425.

Soriano, P., Montgomery, C., Geske, R., and Bradley, A. (1991). Targeted disruption of the c-src proto-oncogene leads to osteopetrosis in mice. Cell *64*, 693–702.

Stein, P. L., Vogel, H., and Soriano, P. (1994). Combined deficiencies of Src, Fyn, and Yes tyrosine kinases in mutant mice. Genes Dev. *8*, 1999–2007.

Subtil, A., and Dautry-Varsat, A. (1997). Microtubule depolymerization inhibits clathrin coated-pit internalization in non-adherent cell lines while interleukin 2 endocytosis is not affected. J. Cell Sci. *110*, 2441–2447.

Suter, D. M., Errante, L. D., Belotserkovsky, V., and Forscher, P. (1998). The Ig superfamily cell adhesion molecule, apCAM, mediates growth cone steering by substrate-cytoskeletal coupling. J. Cell Biol. *141*, 227–240.

Suter, D. M., and Forscher, P. (2001). Transmission of growth cone traction force through apCAM-cytoskeletal linkages is regulated by Src family tyrosine kinase activity. J. Cell Biol. *155*, 427–438.

Suter, D. M., Schaefer, A. W., and Forscher, P. (2004). Microtubule dynamics are necessary for SRC family kinase-dependent growth cone steering. Curr. Biol. *14*, 1194–1199.

Sverdlov, M., Shajahan, A. N., and Minshall, R. D. (2007). Tyrosine phosphorylation-dependence of caveolae-mediated endocytosis. J. Cell Mol. Med. *11*, 1239–1250.

Thomas, S. M., and Brugge, J. S. (1997). Cellular functions regulated by Src family kinases. Annu. Rev. Cell Dev. Biol. *13*, 513–609.

Thomas, S. M., Soriano, P., and Imamoto, A. (1995). Specific and redundant roles of Src and Fyn in organizing the cytoskeleton. Nature *376*, 267–271.

Umemori, H., Sato, S., Yagi, T., Aizawa, S., and Yamamoto, T. (1994). Initial events of myelination involve Fyn tyrosine kinase signalling. Nature *367*, 572–576.

Vallee, R. B. (1982). A taxol-dependent procedure for the isolation of microtubules and microtubule-associated proteins (MAPs). J. Cell Biol. *92*, 435–442.

Vallee, R. B., and Bloom, G. S. (1983). Isolation of sea urchin egg microtubules with taxol and identification of mitotic spindle microtubule-associated proteins with monoclonal antibodies. Proc. Natl. Acad. Sci. USA *80*, 6259–6263.

Wang, D., Huang, X. Y., and Cole, P. A. (2001). Molecular determinants for Csk-catalyzed tyrosine phosphorylation of the Src tail. Biochemistry *40*, 2004–2010.

Woo, S., and Gomez, T. M. (2006). Rac1 and RhoA promote neurite outgrowth through formation and stabilization of growth cone point contacts. J. Neurosci. *26*, 1418–1428.

Xu, W., Doshi, A., Lei, M., Eck, M. J., and Harrison, S. C. (1999). Crystal structures of c-Src reveal features of its autoinhibitory mechanism. Mol. Cell *3*, 629–638.

Yamada, T., Aoyama, Y., Owada, M. K., Kawakatsu, H., and Kitajima, Y. (2000). Scraped-wounding causes activation and association of C-Src tyrosine kinase with microtubules in cultured keratinocytes. Cell Struct. Funct. *25*, 351–359.

E08-06-0603 Suter

Supplemental Figures

Figure S1. *Aplysia* Src1 and Src2 belong to two distinct subfamilies of invertebrate Src PTKs

Phylogenetic tree analysis of *Aplysia californica* (Ap) Src1 (green box) and Src2 (red box) together with selected vertebrate and invertebrate Src family kinases. Calculated distance values in parenthesis; scale bar indicates 0.01. *Asterina miniata* (Am) SFK1 (Accession # AAS01045); *Caenorhabditis elegans* (Ce) Src1 (NP_490866); Ce Src2 (NP_493502); *Drosophila melanogaster* (Dm) Src42A (AAF57295); Dm Src64B (P00528); *Ephydatia fluviatilis* (Ef) Src2 (BAB82421); Ef Src45 (BAB82422); *Gallus gallus* (Gg) Fyn (Q05876); Gg Src (P00523); Gg Yes (P09324); *Homo sapiens* (Hs) Fyn (P06241); Hs Src (P12931); Hs Yes (P07947); *Hydra vulgaris* (Hv) STK (P17713); *Monosiga ovata* (Mo) SrcF (BAF02918); *Suberites domuncula* (Sd) SRC1 (AAT67599); Sd SRC2 (AAT67600); *Spongilla lacustris* (Sl) SRK1 (P42686); *Strongylocentrotus purpuratus* (Sp) Src (NP_999783); *Tribolium castaneum* (Tc) Src (XP_969129).

Figure S2. Specificity of *Aplysia* Src1 and Src2 antibodies.

(A) Cell lysates from CHO cells expressing Src1-EGFP, Src1, Src2-EGFP or Src2, plus untransfected control cells were separated on 10% SDS-PAGE and immunoblotted with Src1, Src2, pSrc2 (activated Src2) or Src PY418 antibodies. No cross reactivity between Src1 and Src2 antibodies was observed. The Src PY418 antibody used in previous studies (Suter and Forscher, 2001; Suter *et al.*, 2004) specifically detects active Src2, but not Src1. 50 and 75 kD molecular weight markers are indicated. (B) Each Src1, Src2 and pSrc2 antibody detects a single band with

the appropriate molecular weight in *Aplysia* CNS cell lysates. Antibodies were either not preincubated (-) or with 5 mg/ml peptide in PBS (+). Peptide incubation completely prevented the detection of the respective Src bands. The phosphorylated peptide (phospho) of Src2, but not the non-phosphorylated peptide (non-phospho) blocked the detection of activated Src2. Molecular weight standards are indicated. (C) *Aplysia* CNS tissue was incubated with lysis buffer (untreated) or lysis buffer including 0.1 % DMSO, 25 μM of the Src family-selective inhibitor PP2, or 25 μM PP3 (inactive PP2 analog) for 20 min. Pretreatment with PP2 resulted in a 54 % decrease of relative Src2 activation levels when compared to the untreated samples (n=2; $P<0.005$, asterisk). In addition, the autophosphorylation mutant of Src2 (Y407F) expressed in SYF cells had relative pSrc2 signals that were reduced by 93% when compared to wild type Src (unpublished data). These results suggest that the pSrc2 antibody is a specific tool to detect activated Src2.

Figure S3. Specificity of *Aplysia* Src1 and Src2 antibodies for immunofluorescence

(A-C) Src1-immunolabeling of fixed *Aplysia* growth cones where Src1 antibody was directly applied (A) or preincubated with 5 mg/ml Src1 peptide (B). Src1-signals in the P domain were reduced by 40% after preincubation with Src1 peptide when compared to controls (n=37 growth cones), while no reduction was observed with the Src2 peptide (data not shown). (C) No Src signals were detected when the primary antibody was omitted in the staining. (D-F) Src2-immunolabeling of growth cones where Src2 antibody was directly applied (D) or preincubated with 5 mg/ml Src2 peptide (E). Src2-signals were reduced by 46% after preincubation with Src2 peptide (n=26 growth cones), while no reduction was observed with the Src1 peptide (data not shown). (F) No signals were detected without the primary antibody. (G-I) pSrc2-immunolabeling

of growth cones where the pSrc2 antibody was directly applied (G) or preincubated with 5 mg/ml pSrc2 phospho peptide (H). pSrc2-signals were reduced by 54% after preincubation with pSrc2 phospho peptide (n=6 growth cones), while no reduction was observed with the corresponding non-phospho peptide (data not shown). (I) Again, no signals were detected when the primary antibody was left out. A dashed line in (C), (F) and (I) indicates the leading edge of the growth cone. Bars: 10 μm.

Figure S4. Src2-EGFP construct validation

(A) Schematic of Src1- and Src2-EGFP fusion protein constructs used in the present study. (B, C) Structural modeling of the *Aplysia* Src2-EGFP fusion protein in inactive (B) and active (C) forms based on known structure of a GFP variant (PDB# 1EMM), the inactive (PDB# 2SRC) and active (PDB# 1Y57) structures of human Src without the first 86 N-terminal amino acids. In its inactive state, the SH2 domain interacts with the phosphorylated tail tyrosine, and the SH3 domain interacts with both the SH2 and kinase domains. Structural modeling suggests that the linker is long and flexible enough to allow tail regulation in the presence of the EGFP-tag. (D) Western blot analysis of Src2 activation state of wild type Src2 and various Src2 mutants with and without EGFP-tag after expression in Sf9 cells. Sf9 cell lysates were separated on 10% SDS-PAGE (15 μg of protein per lane) and the same membrane was sequentially probed with rabbit anti-pSrc2 antibody (immunoblot (IB): pSrc2 to detect autophosphorylated Src2), goat anti-Src2 antibody (IB: Src2 to detect total Src2) and mouse anti-α tubulin antibody (IB: tubulin as a loading control). The Src2 activation state was determined as the ratio between the pSrc2 and total Src2 signal. While the membrane-defective (G2A) and kinase dead (K286M) mutants had a significantly reduced activation level, the constitutively active mutant (Y518F) was similar to

wild type Src2, independent of the presence of EGFP-moiety. Molecular weight markers are indicated. (E) Quantification of two independent experiments by densitometry and determination of the pSrc2/total Src2 ratio revealed that the G2A mutant was at 26±0.3% (mean value ± SD, P=0.002, asterisk) and the K286M mutant was at 13±3.9% (P=0.02) of the wild type Src2 activation level, whereas the constitutively active tail mutant was not significantly different from wild type Src2 (P=0.60). Similarly, the EGFP fusion proteins of the G2A and K286M mutants were at 25±2.7% (P=0.02) and 14±4.6% (P=0.02) of the wild type Src2 activation level, respectively, while Src2-EGFP (P=0.76) and the tail mutant Y518F-EGFP (P=0.47) were not significantly different from wild type Src2. The same results were observed when expressing these constructs in SYF cells (unpublished data).

Figure S5. Src1- and Src2-EGFP FRAP

(A) Src1-EGFP FRAP. A 10 μm diameter bleach spot was made in the P domain of a growth cone with a 20 mW 488 nm argon laser for 10 s. Images shown were taken at times indicated: before bleaching, immediately after bleaching (t= 0s), 5s and 40s after bleaching. (B) Src2-EGFP FRAP. Bars: 10 μm. (C-D) FRAP recovery curves of Src1- and Src2-EGFP. Fluorescence intensity values are plotted as % of pre-bleach intensity and are average values plus SEM from 6-8 experiments in each case. Diffusion constants (D) are indicated.

Figure S6. Constitutively active Src2 does not associate with endocytic vesicles

(A) Growth cone expressing Src2 Y518F-EGFP exhibits constitutively active Src2 at the plasma membrane and filopodia tips but not in distinct vesicles undergoing linear motion as observed for wild type Src2 (see related Video 7). Intensity fluctuations observed are most likely due to ruffling activity (Video 7). (B) Timelapse montage (10 sec intervals) of C domain region marked in (A) shows vesicle labeled with Texas Red dextran, but not with Src2 Y518F-EGFP, moving retrogradely in the C domain. Bar in (A): 10 μm.

Supplemental Videos

Video 1.mov

Time lapse movie of Src2-EGFP-expressing growth cone (Figure 4A). Arrowhead points at Src2-positive puncta structure in the T zone moving first anterogradely, then retrogradely. Time compression: 30x. Scale bar: 10 μm.

Video 2.mov

Time lapse movie of Src2-EGFP-expressing growth cone (Figure 4A). Arrowhead points at Src2-positive puncta structure in the P domain moving retrogradely. Time compression: 30x. Scale bar: 10 μm.

Video 3.mov

Time lapse movie of Src2-EGFP-expressing growth cone (Figure 4C). Red arrowhead points at Src2-positive tubulovesicular structure in the C domain moving retrogradely. Time compression: 30x. Scale bar: 10 μm.

Video 4.mov

Time lapse movie of Src2-EGFP and MT dynamics in *Aplysia* growth cone using FSM (Figure 5G). Yellow arrowhead points at Src2-positive puncta structure (green) in the P domain moving retrogradely in concert with a MT speckle (red). Time compression: 30x. Scale bar: 10 μm.

Video 5.mov

Time lapse movie of Src2-EGFP and MT dynamics using FSM (montage in Figure 5H). Src2-positive puncta structure (green) in the P domain moving retrogradely in concert with a MT speckle (red). Time compression: 30x. Scale bar: 1 μm.

Video 6.mov

Time lapse movie of Src2-EGFP-positive tubulovesicular structures in the C domain before (in 0.1% DMSO) and after 1 hour treatment with 5 μM nocodazole. 5 minute duration is shown for both DMSO and nocodazole treatment. Note absence of dynamic Src2-positive organelle, reduced leading edge motility and increased Src2 levels after nocodazole treatment. Time compression: 60x. Scale bar: 10 μm.

Video 7.mov

Time lapse movie of Src2 Y518F-EGFP-expressing growth cone shows constitutively active Src2 is enriched in tips of long filopodia (arrowhead). Note the clear absence of linear movements of distinctly labeled Src2 Y518F-EGFP-positive vesicles in any of the growth cone domains. Time compression: 100x. Scale bar: 10 μm.

Supplemental Table S1. Primers used for cloning of Aplysia Src1 and Src2

A) Degenerate primers used for initial PCR reactions

Function	*Sequence*
Forward primer G130-A138 of chicken Src	5'-GGITAYATYCCITCIAAYTAYGTNGC-3'
Reverse primer F278-N287 of chicken Src	5'-TTCCAIGTICCCATCCAIACYTCICCRAA-3'
Reverse primer E332-M341 of chicken Src	5'-CATRTAYTCIGTIACRATRTARATIGGYTC-3'

B) Primers for 5' and 3' RACE reactions

Function	*Sequence*
Nested 5' Src1 RACE primer	5'-GTGGCGTGGCATCGTCCTTGGCTACATAA-3'
5' Src1 RACE primer	5'-CACGCCGCTCCCAGCTGACAGCACAGG-3'
3' Src1 RACE primer	5'-GGCAACCCTCGCGGAACTTTCCTGGTCAGAG-3'
Nested 3' Src1 RACE primer	5'-GGCCCACCGTCCAGTTCCGAGAGC-3'
Nested 5' Src2 RACE primer	5'-GATCTCCCACTGATCTTTTGTGTTGTACGACAGAC-3'
5' Src2 RACE primer	5'-GGTGTGGTGTTGTTCCAAAGACCCTCCCAAACTTC-3'
3' Src2 RACE primer	5'-CAGTCCGTGATGGAGACACAGTCAAACATTACAGA-3'
Nested 3' Src2 RACE primer	5'-GTCATGGGCAGTTTGGAGAAGTTTGGGAGGG-3'

C) Primers for Src1 and Src2 subcloning into pRAT-EGFP vector

Function	*Sequence*
Forward primer Src1	5'-CTATGCACCGGTCGCCACCATGGGCAACCTGTGCGTGAAAG-3'
Reverse primer Src1	5'-ACTGGCAACCGGTCCTCCTCCTCCTCCACGACTAATATCGTCCATCTC-3'
Forward primer Src2	5'-GTATGCACCGGTCGCCACCATGGGTAACTGCTTCGGGGGA-3'
Reverse primer Src2	5'-ACTGGCAACCGGTCCTCCTCCTCCTCCTCGTATGAAAGAGGCCTCTCT-3'

D) Primers for Src1 and Src2 subcloning into pRAT vector

Function	*Sequence*
Forward primer Src1	5’-CTACTCGAATTCCGCCACCATGGGCAACCTGTGCGTGAAAG-3’
Reverse primer Src1	5’-GCTGCGGGAATTCTCAACGACTAATATCGTCCATCTC-3’
Forward primer Src2	5’-CAAATCCGCGGCGCCACCATGGGTAACTGCTTCGGGG-3’
Reverse primer Src2	5’-GCGTCTCCGCGGTTATCGTATGAAAGAGGCCTCTCT-3’

E) Primers for Src1 and Src2 subcloning into pIZV5-6His vector

Function	*Sequence*
Forward primer Src1	5’-ACACACACTAGTACTCCACCATGGGCAACCTGTGCGTGAAAG-3’
Reverse primer Src1	5’-ATAGATCTCGAGCGACGACTAATATCGTCCATCT-3’
Forward primer Src2	5’-ACACACACTAGTACTCCACCATGGGTAACTGCTTCGGGGGAT-3’
Reverse primer Src2	5’-ATAGATCTCGAGCGTCGTATGAAAGAGGCCTCTC-3’

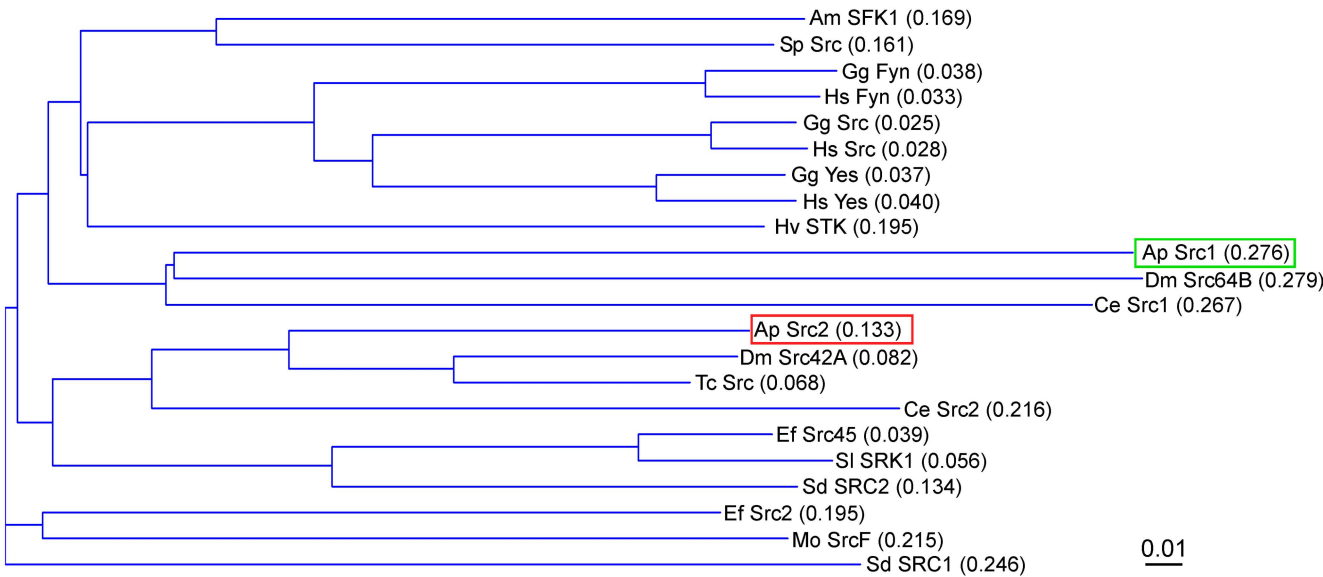

Supplemental Figure S1; Wu et al.

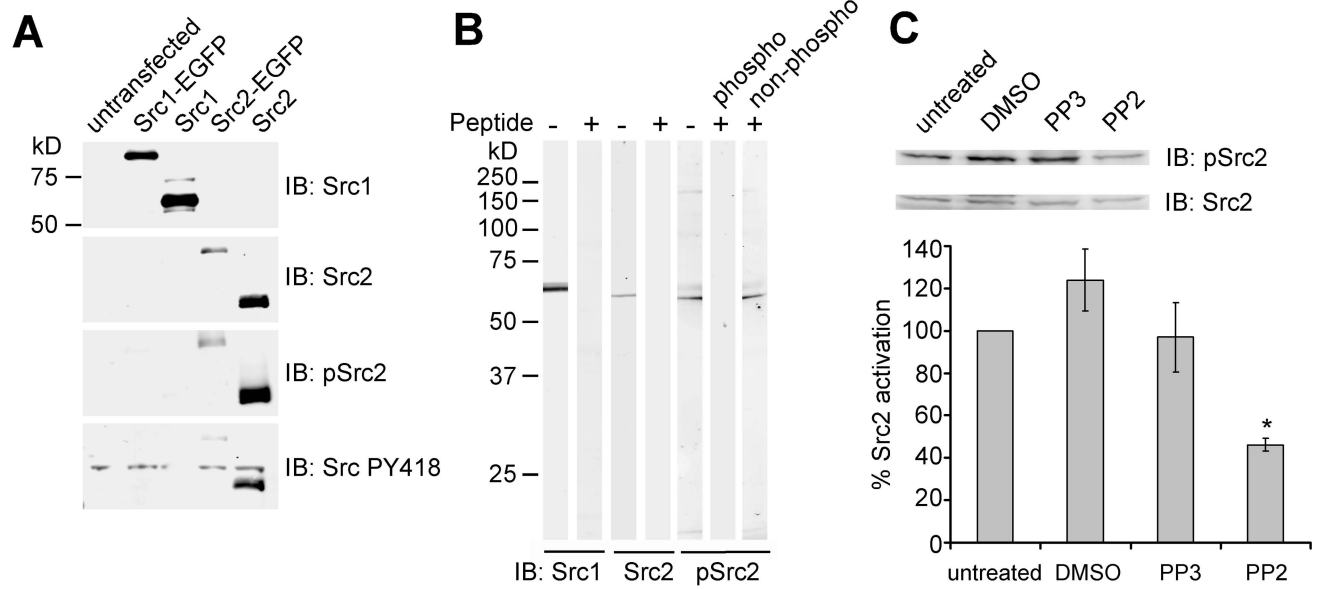

Supplemental Figure S2; Wu et al.

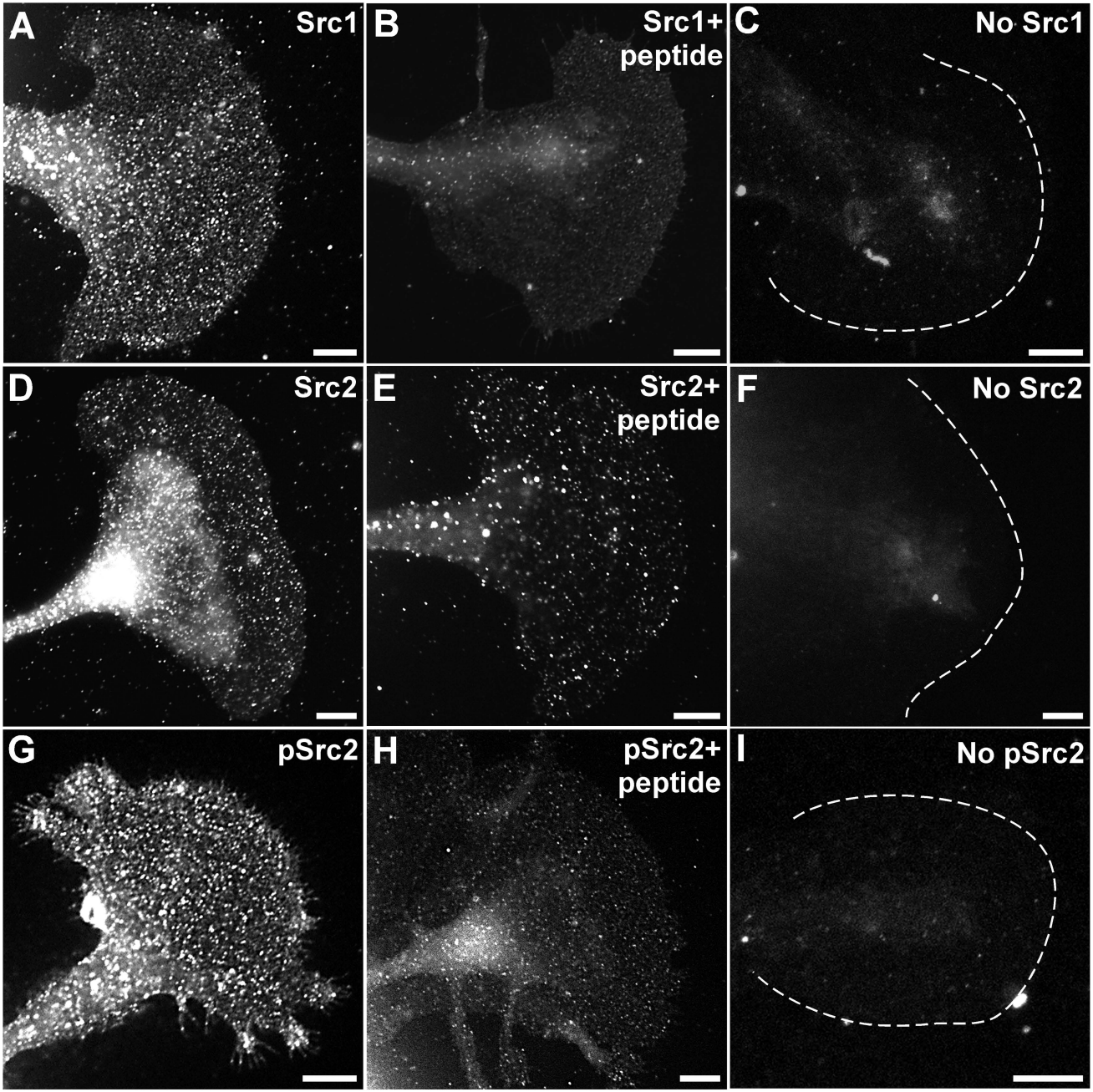

Supplemental Figure S3; Wu et al.

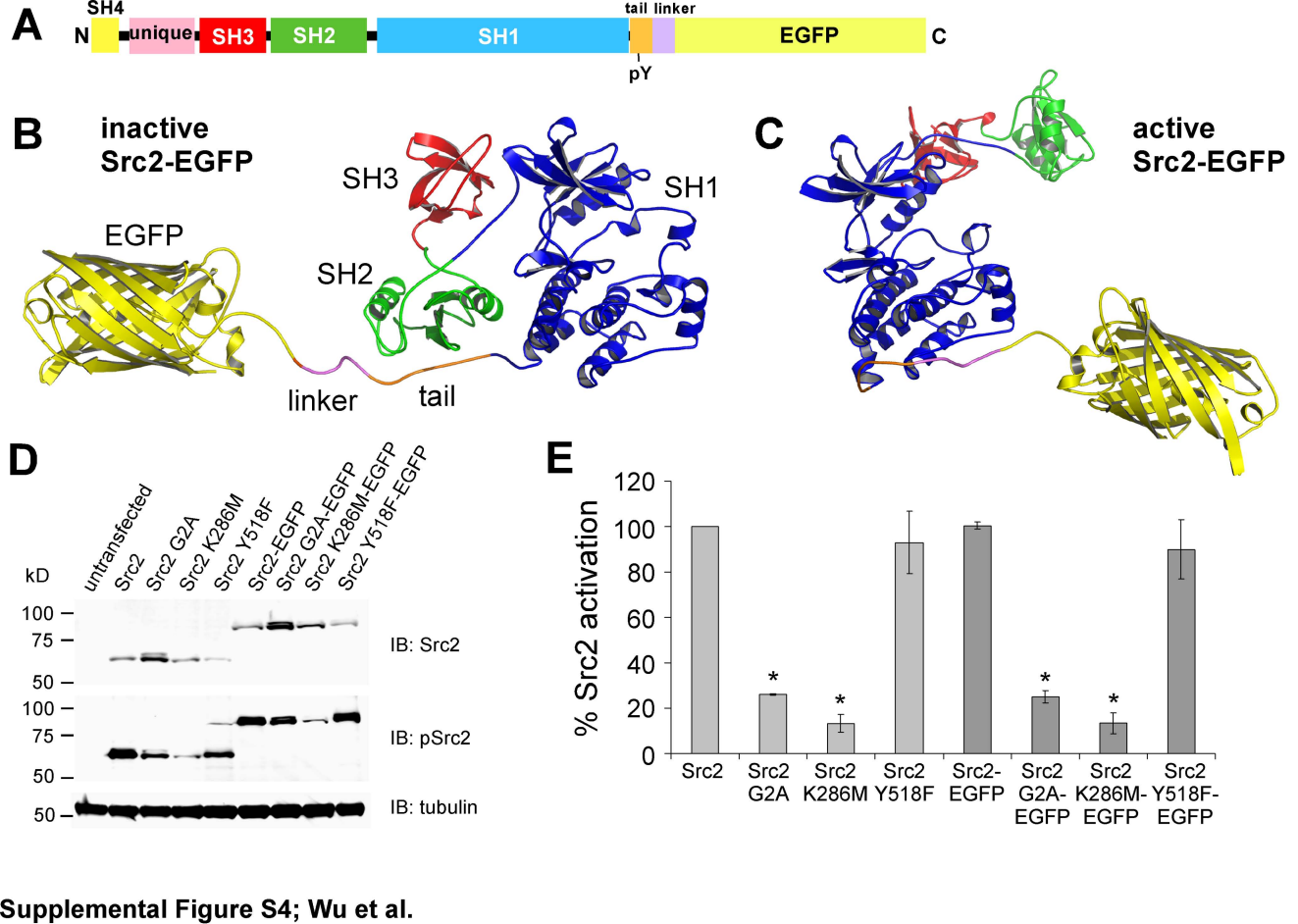

Supplemental Figure S4; Wu et al.

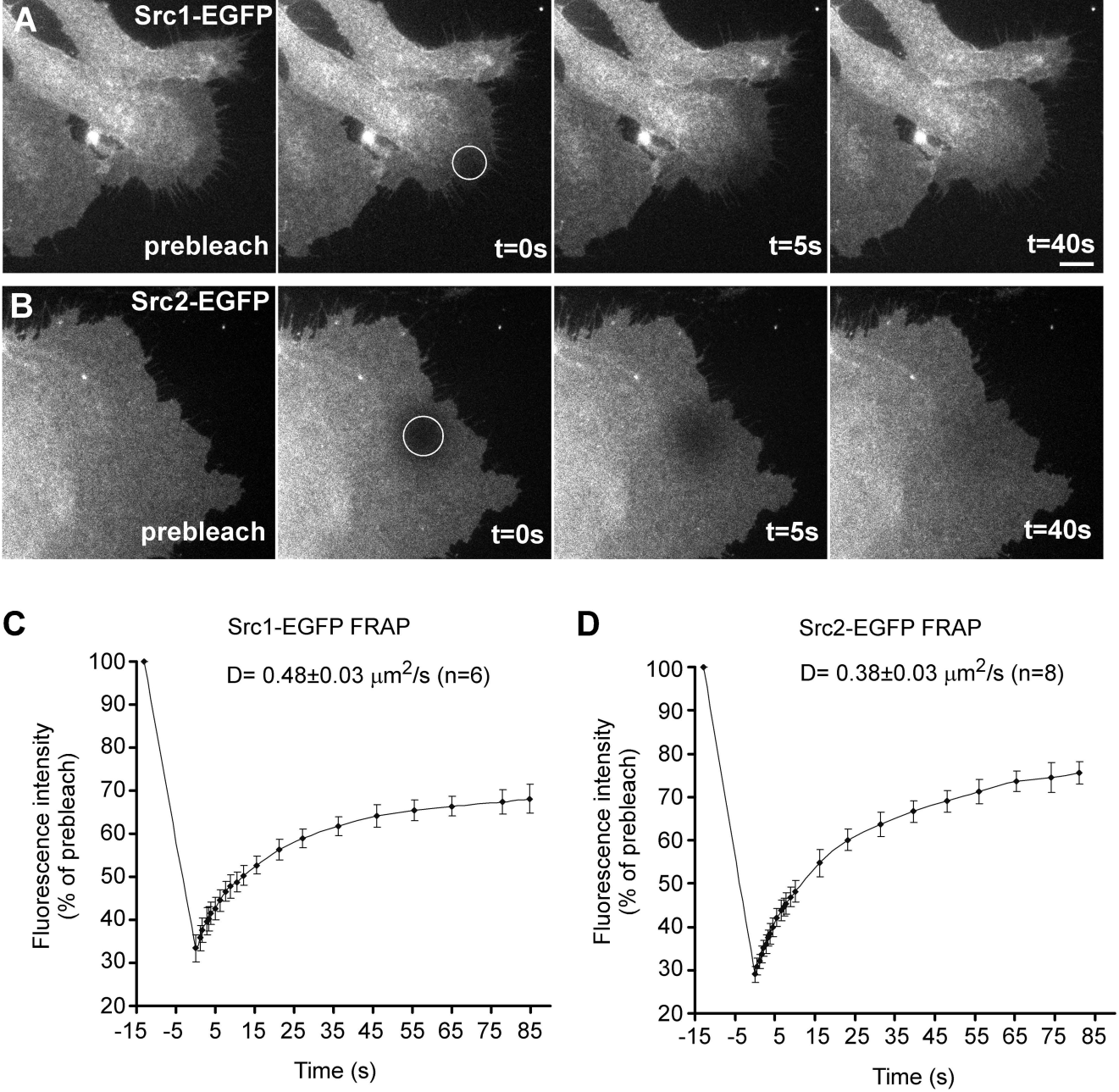

Supplemental Figure S5; Wu et al.

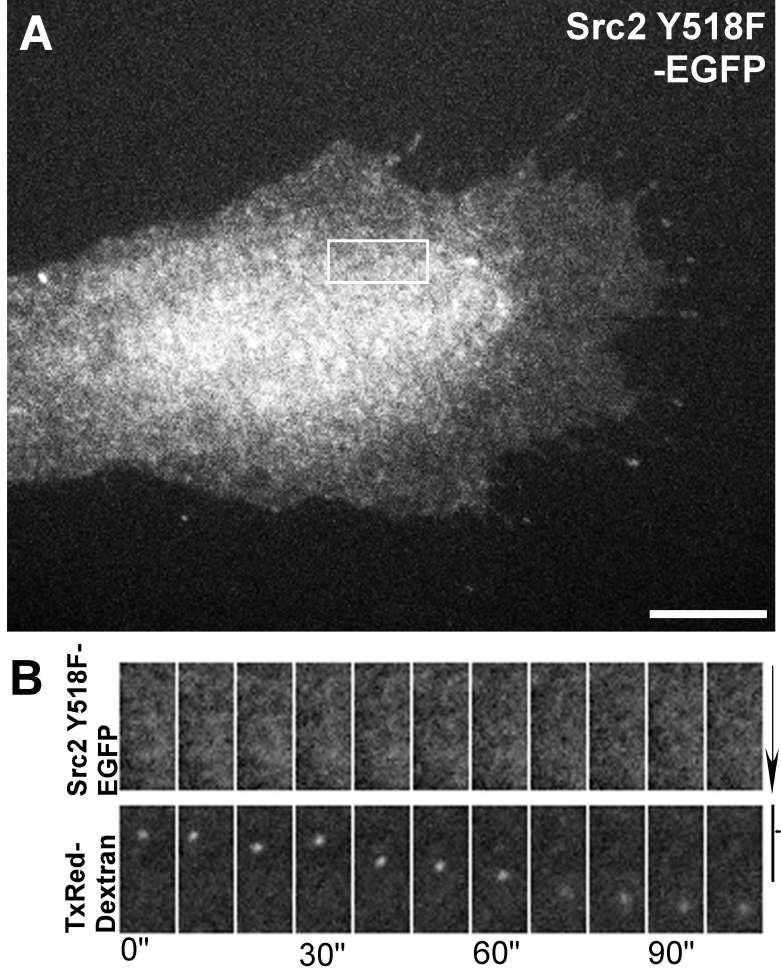

Supplemental Figure S6; Wu et al.